AGU PUBLICATIONS

Paleoceanography and Paleoclimatology

RESEARCH ARTICLE
10.1002/2017PA003174

**Key Points:**
- Published and new deep ocean radiocarbon records for the past 40 kyr are compiled
- A 16-box model of modern ventilation is fit to the deglacial data
- The residuals of the fit can generally be explained by data uncertainties

**Supporting Information:**
- Supporting Information S1

**Correspondence to:**
N. Zhao,
nzhao@whoi.edu

**Citation:**
Zhao, N., Marchal, O., Keigwin, L., Amrhein, D., & Gebbie, G. (2018). A synthesis of deglacial deep-sea radiocarbon records and their (in) consistency with modern ocean ventilation. *Paleoceanography and Paleoclimatology*, *33*, 128–151. https://doi.org/10.1002/2017PA003174

Received 2 JUN 2017
Accepted 23 DEC 2017
Accepted article online 8 JAN 2018
Published online 3 FEB 2018



# A Synthesis of Deglacial Deep-Sea Radiocarbon Records and Their (In)Consistency With Modern Ocean Ventilation

**Ning Zhao[1,2], Olivier Marchal[3], Lloyd Keigwin[3], Daniel Amrhein[4], and Geoffrey Gebbie[5]**

[1]Massachusetts Institute of Technology-Woods Hole Oceanographic Institution Joint Program in Oceanography, Woods Hole, MA, USA, [2]Now at Climate Geochemistry Department, Max Planck Institute for Chemistry, Mainz, Germany, [3]Department of Geology and Geophysics, Woods Hole Oceanographic Institution, Woods Hole, MA, USA, [4]School of Oceanography and Department of Atmospheric Sciences, University of Washington, Seattle, WA, USA, [5]Department of Physical Oceanography, Woods Hole Oceanographic Institution, Woods Hole, MA, USA

**Abstract** We present a synthesis of 1,361 deep-sea radiocarbon data spanning the past 40 kyr and computed (for $^{14}$C-dated records) from the same calibration to atmospheric $^{14}$C. The most notable feature in our compilation is a long-term $\Delta^{14}$C decline in deep oceanic basins over the past 25 kyr. The $\Delta^{14}$C decline mirrors the drop in reconstructed atmospheric $\Delta^{14}$C, suggesting that it may reflect a decrease in global $^{14}$C inventory rather than a redistribution of $^{14}$C among different reservoirs. Motivated by this observation, we explore the extent to which the deep water $\Delta^{14}$C data jointly require changes in basin-scale ventilation during the last deglaciation, based on the fit of a 16-box model of modern ocean ventilation to the deep water $\Delta^{14}$C records. We find that the fit residuals can largely be explained by data uncertainties and that the surface water $\Delta^{14}$C values producing the fit are within the bounds provided by contemporaneous values of atmospheric and deep water $\Delta^{14}$C. On the other hand, some of the surface $\Delta^{14}$C values in the northern North Atlantic and the Southern Ocean deviate from the values expected from atmospheric $^{14}CO_2$ and $CO_2$ concentrations during the Heinrich Stadial 1 and the Bølling-Allerød. The possibility that deep water $\Delta^{14}$C records reflect some combination of changes in deep circulation and surface water reservoir ages cannot be ruled out and will need to be investigated with a more complete model.

## 1. Introduction

Variations in the exchange of $CO_2$ between the ocean and the atmosphere have long been postulated to have contributed to the preindustrial changes in the concentration of atmospheric $CO_2$ documented in Antarctic ice core records (e.g., Knox & McElroy, 1984; Sarmiento & Toggweiler, 1984; Siegenthaler & Wenk, 1984). Among the processes that could modify air-sea $CO_2$ fluxes on centennial and longer time scales resolved by these records are changes in ocean circulation, particularly in the transport between surface and deep waters. These changes could modify the temperature, salinity, dissolved inorganic carbon, and alkalinity of surface waters, thereby altering surface water $CO_2$ partial pressure and air-sea $CO_2$ flux (Sarmiento & Gruber, 2006). In particular, the Southern Ocean, where transport of deep waters to the surface would be favored by upwelling along density surfaces, has been suggested to be an important region for understanding past changes in atmospheric $pCO_2$ (for recent reviews, see Fischer et al., 2010; Sigman et al., 2010) and climate (Marshall & Speer, 2012). Indeed, circulation changes in the Southern Ocean have been inferred from a variety of paleoclimatic indicators (e.g., Anderson et al., 2009; Jaccard et al., 2016; Schmitt et al., 2012; Skinner et al., 2010).

In paleoceanography, quantitative information about the exchange between surface and deep waters is often deduced from the "age" of deep waters relative to that of the surface waters or the atmosphere (for recent studies, see, e.g., Burke & Robinson, 2012; Chen et al., 2015; Freeman et al., 2016; Keigwin & Lehman, 2015; Rae et al., 2014; Sikes et al., 2016; Skinner et al., 2015). The age of deep ocean waters over the past 40 kyr or so is typically estimated from measurements of the radiocarbon (half-life of 5,700 ± 30 years; Audi et al., 2003) activity of fossil samples of benthic foraminifera or deep-dwelling corals. Many studies relied on such measurements to draw inferences about deep ocean "ventilation" during the last deglaciation, a period during which the atmospheric $CO_2$ concentration is estimated to have increased by about 80 ppmv (e.g., Monnin et al., 2001). Notably, Marchitto et al. (2007) and Bryan et al. (2010) suggested that Antarctic

Intermediate Water (AAIW) was significantly older than today during the Heinrich Stadial 1 (HS1, circa 17.6–14.7 kyr B.P.) and the Younger Dryas (YD, circa 12.9–11.7 kyr B.P.) using sediment cores from the eastern North Pacific and the northern Indian Ocean, respectively. Both studies argued that the inferred presence of low $^{14}C$ concentration in AAIW during these two intervals was due to increased ventilation of Southern Ocean deep waters that would have released carbon accumulated at abyssal depths during the last glacial period into the overlying AAIW and the atmosphere.

This interpretation, however, has not gone unchallenged. Samples from the eastern South Pacific (De Pol-Holz et al., 2010) and western South Pacific (Rose et al., 2010) do not support an aging of AAIW during the HS1 and the YD. Moreover, there is debate over whether an isolated, deep ocean reservoir existed during the Last Glacial Maximum (LGM), a time interval centered at circa 21 kyr B.P. On the one hand, samples from several ocean basins suggest the presence of relatively old deep waters during the LGM, for example, in the eastern Equatorial Pacific (Keigwin & Lehman, 2015), the western South Pacific (Sikes et al., 2016), and the Atlantic sector of the Southern Ocean (Skinner et al., 2010). On the other hand, some studies concluded that the ages of deep ocean waters during the LGM were not substantially different from today (e.g., Broecker et al., 2004; Broecker & Clark, 2010; Lund et al., 2011). In the same vein, model calculations tend to challenge the notion that exchange with an isolated deep ocean reservoir produced the $^{14}C$ activity drop observed at intermediate depths during the last deglaciation (e.g., Hain et al., 2011).

Many factors can influence a particular deep ocean radiocarbon record in addition to basin-scale changes in bottom water age. For instance, estimating the initial radiocarbon concentration (usually expressed as $\Delta^{14}C$, the $^{14}C/^{12}C$ ratio referred to a preindustrial atmospheric value and corrected for isotopic fractionation) of a fossil sample of benthic foraminifera or deep-sea coral requires accurate knowledge about the calendar age of the sample. The calendar ages of such samples, however, can suffer from various uncertainties due, for example, to the post-depositional movement of foraminiferal shells along the sedimentary column (bioturbation), changes in the difference in $^{14}C$ ages between the ocean surface water and the atmosphere (reservoir age), and gains or losses of U-series isotopes in corals (open-system behavior; e.g., Robinson et al., 2006). Each of these sources of uncertainty can lead to a sizeable error in the reconstructed value of bottom water $\Delta^{14}C$. In general, the errors in calendar chronology and hence in bottom water $\Delta^{14}C$ tend to be larger for older samples.

Other factors compound the interpretation of deep-sea radiocarbon records in terms of bottom water age. For example, changes in the radiocarbon age of ocean bottom water may not necessarily reflect changes in the true age of the water, since the radiocarbon concentration of waters entering the deep sea may vary with time (e.g., Wunsch, 2003). Mixing between different water masses is also likely to bias age estimates deduced from radiocarbon ages, as radiocarbon concentration is a nonlinear function of radiocarbon age. Finally, inferences made from single records, which constitute the majority of the literature on the subject, often assume that changes observed in the record are representative of a large oceanic region. However, single records may not represent basin-scale changes of bottom water age in a straightforward manner, especially if they originate from a region characterized by large gradients in radiocarbon concentration. The above considerations suggest that an analysis of multiple records which gives due consideration to errors is needed for a rigorous interpretation of deep-sea radiocarbon data in terms of paleoceanographic events.

In this study, we report a compilation of deep water $\Delta^{14}C$ estimates for the last 40 kyr and examine the compiled data in the presence of a simple (box) model of modern ocean ventilation. Specifically, we explore the extent to which deglacial radiocarbon records from different oceanic basins jointly require changes in basin-scale ventilation during this period, given their errors and their scarcity (by modern standards). To this end, the model of modern ocean ventilation is fit to the deep water $\Delta^{14}C$ records, and we examine whether (i) the differences between the observed and fitted values of deep water $\Delta^{14}C$ are larger than the uncertainties and (ii) the surface water $\Delta^{14}C$ values implied by the fit lie outside of upper or lower bounds. The upper bound is provided by the reconstructed value of contemporaneous atmospheric $\Delta^{14}C$ (Reimer et al., 2013): since $^{14}C$, a cosmogenic radionuclide, is produced in the atmosphere, $\Delta^{14}C$ in surface water is expected to be always smaller than atmospheric $\Delta^{14}C$, although pathological cases where surface ocean $\Delta^{14}C$ is higher than atmospheric $\Delta^{14}C$ could be constructed. The lower bound is provided by the contemporaneous $\Delta^{14}C$ values that are found in the deep ocean. Although factors such as a larger sea ice extent could increase

reservoir ages and decrease surface water $\Delta^{14}C$ in high-latitude regions (e.g., Bard, 1988), the lowest $\Delta^{14}C$ values in the ocean are expected to occur at depth rather than near the surface.

This paper is organized as follows. In section 2, we describe (i) our compilation of published and new deep water radiocarbon data, (ii) the treatment of these data for the present analysis, (iii) the box model of modern ocean ventilation, and (iv) the method used to fit the model to the data. The results of our analysis are presented in section 3. In section 4, we discuss their sensitivity to various assumptions about the data and the model. We clarify their paleoceanographic implications in section 5. Finally, possible perspectives of research are mentioned in section 6.

It is worth being explicit about the limitations of this study. One obvious limitation arises from the spatial distribution and scarcity (by modern standards) of deep water $\Delta^{14}C$ data. The spatial distribution and scarcity of the data may bias inferences of past ocean conditions, although an effort is made to account for the resulting uncertainties (section 2.1). Likewise, the temporal resolution of radiocarbon records is relatively poor, implying that centennial and higher frequency variability is typically not resolved and may alias onto longer-period changes. Also, as alluded to above, estimates of paleo-$\Delta^{14}C$ of deep ocean waters suffer from significant uncertainties, such as due to chronological errors. In this study, we rely on the sediment and coral chronologies reported in the original publications and conduct recalibration according to IntCal13 (Reimer et al., 2013), if needed. It is thus expected that unrecognized errors in the chronologies and in the IntCal13 calibration, in particular, systematic errors, would influence our results to some extent. Another limitation resides in the very coarse resolution of the model that is used to interpret the data. Although use of a very coarse resolution model is consistent with our research question and benefits from simplicity of interpretation, it implies that the paleodata be averaged over large oceanic volumes and that the errors in the volume averages be properly estimated. Support for our approach to derive basin-scale $\Delta^{14}C$ from $\Delta^{14}C$ measurements on fossil carbonates from a few sites is reported in section 3.1. Despite the aforementioned limitations, the present investigation appears justified given the postulated role of basin-scale ocean circulation changes in deglacial variations of atmospheric $pCO_2$ and climate.

## 2. Methods

### 2.1. Deep Water Radiocarbon Data

The sources of the deep water radiocarbon data compiled for this study are listed in Table 1, where the data appear in order of decreasing latitude. Our compilation (available at the National Climatic Data Center of NOAA; https://www.ncdc.noaa.gov/paleo/study/21390) includes data published until December 2016 as well as our new data (Table 1). Overall, it comprises a total number of 1,361 deep water $^{14}C$ age estimates for the past 40 kyr based on $^{14}C$ measurements on fossil samples of benthic foraminifera (76.0% of the data), deep-dwelling corals (23.0%), deep-dwelling planktonic foraminifera (0.6%), and bivalves and spiral shells (0.4%). The geographic distribution of the data is very irregular: most of the samples originate from near the oceanic margins, and large oceanic regions are devoid of any data (e.g., the South Indian Ocean; Figure 1). The depths of the samples vary from about 250 m to 5,000 m (Figure S1 in the supporting information). Approximately 55% of the samples come from depths greater than 1,500 m, and only about 25% of the samples come from depths greater than 2,500 m. Factors contributing to the depth distribution include the difficulty in obtaining carbonate material for paleoceanographic reconstruction in deep, corrosive water, and the small number of corals dredged below about 2,500 m.

In contrast to most other paleoceanographic indicators, the magnitude of a $\Delta^{14}C$ estimate is a function of the sample calendar age, as this is used to correct for radioactive decay until the time of sample collection. In our compilation, the calendar ages of benthic foraminiferal samples used to reconstruct bottom water $\Delta^{14}C$ are generally based on (i) $^{14}C$ dates of co-occurring planktonic foraminifera in the core, (ii) estimates of surface water reservoir age, and (iii) the relationship between atmospheric $^{14}C$ and calendar ages ($^{14}C$ calibration; e.g., Reimer et al., 2013). Samples associated with apparent age reversal or loose age constraints are excluded from our compilation (e.g., planktonic foraminiferal or ash age from an asynchronous deposition layer could introduce significant dating errors for cores with low sedimentation rates). For some other benthic foraminiferal samples, calendar ages have been determined from assumptions about phase relationships with other, relatively well-dated records ("wiggle matching"). The calendar ages of deep-dwelling corals, on the other hand, are typically established from $^{234}U/^{230}Th$ dates and the assumption of closed system. Calendar ages

**Table 1**
*List of Deep Water $\Delta^{14}C$ Data Compiled in This Study (BF: Benthic Foraminifera; DC: Deep-Dwelling Coral; PF: Planktonic Foraminifera)*

| Latitude | Longitude | Sediment core/coral name | Modern water depth (m) | Substrate | References |
|---|---|---|---|---|---|
| 63.0 | −17.6 | RAPiD-10-1P | 1,237 | BF | Thornalley et al. (2011) |
| 62.3 | −17.1 | RAPiD-15-4P | 2,133 | BF | Thornalley et al. (2011) |
| 61.5 | −19.5 | RAPiD-17-5P | 2,303 | BF | Thornalley et al. (2011) |
| 60.1 | −179.4 | SO202-18-6 | 1,100 | BF | Max et al. (2014) |
| 59.6 | −144.2 | EW0408-84TC | 682 | BF | Davies-Walczak et al. (2014) |
| 58.9 | 170.7 | SO201-2-101KL | 630 | BF | Max et al. (2014) |
| 57.5 | 170.4 | SO201-2-85KL | 968 | BF | Max et al. (2014) |
| 56.3 | 170.7 | SO201-2-77KL | 2,135 | BF | Max et al. (2014) |
| 55.5 | −15.7 | 2706 | 724 | DC | Schroder-Ritzrau et al. (2003) |
| 54.6 | −148.8 | ODP887 | 3,647 | BF | Galbraith et al. (2007) |
| 54.5 | 144.8 | LV27-2-4 | 1,305 | BF | Gorbarenko et al. (2010) |
| 54.4 | −148.9 | MD02-2489 | 3,640 | BF | Gebhardt et al. (2008); Rae et al. (2014) |
| 54.0 | 162.4 | SO201-2-12KL | 2,145 | BF | Max et al. (2014) |
| 53.7 | 165.0 | VINO19-4 GGC17 | 3,960 | BF | Cook and Keigwin (2015) |
| 52.7 | 144.7 | SO178-13-6 | 713 | BF | Max et al. (2014) |
| 52.2 | −12.8 | 2307 | 686 | DC | Schroder-Ritzrau et al. (2003) |
| 51.3 | 167.7 | MD01-2416 | 2,317 | BF | Sarnthein et al. (2006, 2007) |
| 51.2 | 167.8 | ODP883 | 2,385 | BF | Sarnthein et al. (2006) |
| 51.1 | 167.9 | RNDB GGC5 | 2,804 | BF | Cook and Keigwin (2015) |
| 51.1 | 169.0 | RNDB PC11 | 3,225 | BF | Cook and Keigwin (2015); Keigwin and Lehman (2015) |
| 51.1 | 168.1 | RNDB GGC15 | 3,700 | BF | Cook and Keigwin (2015) |
| 51.0 | 148.3 | 936 | 1,305 | BF | Gorbarenko et al. (2004) |
| 50.4 | −46.4 | Orphan Knoll deep-sea corals | 1,600 | DC | Cao et al. (2007) |
| 50.4 | 167.7 | VINO19-4 GGC37 | 3,300 | BF | Cook and Keigwin (2015) |
| 50.1 | 153.2 | V34-98 | 1,175 | BF | Gorbarenko et al. (2002) |
| 49.7 | 168.3 | RNDB PC13/PG13 | 2,329 | BF | Cook and Keigwin (2015); Keigwin and Lehman (2015) |
| 49.6 | 150.2 | Nesmeyanov25-1 GGC27 | 995 | BF | Keigwin (2002); Cook and Keigwin (2015) |
| 49.4 | 152.9 | LV29-114-3 | 1,765 | BF | Max et al. (2014) |
| 49.1 | 150.3 | B34-91 | 1,227 | BF | Keigwin (2002) |
| 48.9 | −126.9 | JT96-09 | 920 | BF | McKay et al. (2005) |
| 48.9 | 150.4 | Nesmeyanov25-1 GGC20 | 1,510 | BF | Keigwin (2002); Cook and Keigwin (2015) |
| 48.8 | 150.4 | Nesmeyanov25-1 GGC18 | 1,700 | BF | Keigwin (2002); Cook and Keigwin (2015) |
| 48.6 | 150.4 | Nesmeyanov25-1 GGC15 | 1,980 | BF | Keigwin (2002); Cook and Keigwin (2015) |
| 47.6 | −7.3 | 2774 | 490 | DC | Schroder-Ritzrau et al. (2003) |
| 47.0 | −5.5 | 1471 and 2631 | 240 | DC | Schroder-Ritzrau et al. (2003) |
| 44.5 | 145.0 | MR0604 PC04A | 1,215 | BF | Okazaki et al. (2014) |
| 43.5 | −54.9 | OCE326 GGC26 | 3,975 | BF; Bivalve | This study |
| 43.5 | −54.8 | KNR197-10 CDH42 | 3,870 | BF | Keigwin and Swift (2017) |
| 43.4 | −60.2 | KNR197-10 CDH46 | 965 | BF | This study |
| 43.1 | −49.0 | KNR197-10 GGC36 | 1,520 | BF | This study |
| 43.1 | −55.8 | OCE326 GGC14 | 3,525 | BF | Robinson et al. (2005); this study |
| 43.0 | −55.3 | HU73031-7 | 4,055 | BF | Robinson et al. (2005) |
| 43.0 | −59.9 | HU72021-3 | 2,470 | BF | Robinson et al. (2005) |
| 42.2 | 144.2 | GH02-1030 | 1,212 | BF | Ikehara et al. (2006) |
| 42.1 | −125.8 | W8709A-13PC | 2,710 | BF | Mix et al. (1999); Lund et al. (2011) |
| 42.0 | −29.0 | JFA deep-sea corals | 1,684–1,829 | DC | Adkins et al. (1998) |
| 41.7 | 142.6 | CH84-14 | 978 | BF | Duplessy et al. (1989) |
| 41.7 | −124.9 | ODP1019 | 980 | BF | Mix et al. (1999) |
| 41.1 | 142.4 | MR01-K03-PC4/5 | 1,366 | BF | Ahagon et al. (2003) |
| 40.4 | 143.5 | KR02-15-PC6 | 2,215 | BF | Minoshima et al. (2007) |
| 40.0 | −69.0 | KNR198 CDH36 | 1,828 | BF | This study |
| 39.2 | −68.0 | KNR198 GGC15 | 3,308 | BF | This study |
| 34.0–40.0 | −66.0 – −57.0 | New England Seamount deep-sea corals | 1,176–2,529 | DC | Adkins et al. (1998); Robinson et al. (2005); Eltgroth et al. (2006); Thiagarajan et al. (2014) |
| 38.0 | −31.1 | MD08-3180 | 3,064 | BF | Sarnthein et al. (2015) |
| 38.0 | −25.6 | Smithsonian deep-sea coral | 1,069–1,235 | DC | Eltgroth et al. (2006) |

**Table 1** *(continued)*

| Latitude | Longitude | Sediment core/coral name | Modern water depth (m) | Substrate | References |
|---|---|---|---|---|---|
| 37.8 | −10.2 | MD99-2334K | 3,146 | BF | Skinner and Shackleton (2004); Skinner et al. (2010); Skinner et al. (2014) |
| 37.8 | −9.7 | JC89-SHAK-14-4G | 2,063 | BF | Freeman et al. (2016) |
| 37.8 | −9.5 | JC89-SHAK-10-10K | 1,127 | BF | Freeman et al. (2016) |
| 37.7 | −10.5 | JC89-SHAK-03-6K | 3,735 | BF | Freeman et al. (2016) |
| 37.6 | −10.7 | JC89-SHAK-05-3K | 4,670 | BF | Freeman et al. (2016) |
| 37.6 | −10.4 | JC89-SHAK-06-4K | 2,642 | BF | Freeman et al. (2016) |
| 37.2 | −123.2 | F8-90-G21 | 1,605 | BF | van Geen et al. (1996) |
| 37.1 | −31.9 | KNR197-10 GGC5 | 2,127 | BF | This study |
| 36.4 | −48.5 | KNR197-10 GGC17 | 5,011 | BF | Keigwin and Swift (2017) |
| 36.1 | −72.3 | KNR178 GGC2 | 3,927 | BF | Keigwin and Swift (2017) |
| 36.1 | 141.8 | MD01-2420 | 2,101 | BF | Okazaki et al. (2012) |
| 36.0 | −74.7 | KNR178 JPC32 | 1,006 | BF | This study |
| 35.6 | −121.6 | F2-92-P3 | 799 | BF | van Geen et al. (1996) |
| 34.4 | −30.5 | 660 | 795–830 | DC | Schroder-Ritzrau et al. (2003) |
| 34.3 | −120.0 | ODP893A | 576.5 | BF; Bivalve; Spiral Shell | Ingram and Kennett (1995); Sarnthein et al. (2007); Magana et al. (2010) |
| 34.2 | 137.7 | BO04-PC11 | 1,076 | BF | Ikehara et al. (2011) |
| 34.0 | −63.0 | Muir Seamount deep-sea corals | 2,026–2,441 | DC | Robinson et al. (2005); Eltgroth et al. (2006); Thiagarajan et al. (2014) |
| 33.7 | −57.6 | HU89038-8PC | 4,600 | Bivalve | Keigwin and Boyle (2008) |
| 33.7 | −57.6 | OCE326 GGC5 | 4,600 | Bivalve | Keigwin and Boyle (2008) |
| 33.7 | −57.6 | KNR31 GPC5 | 4,583 | BF | This study |
| 33.2 | −29.0 | 654 | 695 | DC | Schroder-Ritzrau et al. (2003) |
| 32.9 | −76.3 | KNR140 GGC56 | 1,400 | BF | Robinson et al. (2005) |
| 32.8 | −76.3 | KNR140 GGC51 | 1,790 | BF | Keigwin (2004); Robinson et al. (2005) |
| 32.8 | −76.2 | KNR140 GGC50 | 1,903 | BF | Keigwin (2004); this study |
| 32.8 | −13.3 | 2657 | 1,284–1,350 | DC | Schroder-Ritzrau et al. (2003) |
| 32.5 | −76.3 | KNR140 GGC66 | 2,155 | BF | Keigwin (2004) |
| 32.4 | −76.4 | KNR140 JPC01 | 2,243 | BF | Keigwin (2004) |
| 32.2 | −76.3 | KNR140 PG02 | 2,394 | BF | Keigwin (2004) |
| 32.2 | 133.9 | KT89-18-P4 | 2,700 | BF | Okazaki et al. (2010) |
| 32.0 | −76.1 | KNR140 GGC43 | 2,590 | BF | Keigwin (2004) |
| 31.7 | −75.4 | KNR140 JPC37 | 2,972 | BF | Keigwin and Schlegel (2002) |
| 31.7 | −75.4 | KNR140 GGC39 | 2,975 | BF | Keigwin and Schlegel (2002) |
| 30.7 | −74.5 | KNR140 GGC30 | 3,433 | BF | Robinson et al. (2005) |
| 29.8 | −12.7 | 2088 | 652–986 | DC | Schroder-Ritzrau et al. (2003) |
| 29.7 | −73.4 | KNR140 GGC26 | 3,845 | BF | Keigwin (2004) |
| 29.1 | −72.9 | KNR140 JPC12 | 4,250 | BF | Keigwin (2004); Robinson et al. (2005); this study |
| 28.3 | −74.4 | KNR140 JPC22 | 4,712 | BF | Keigwin (2004) |
| 27.9 | −111.7 | DSDP 480 | 655 | BF | Keigwin and Lehman (2015) |
| 27.5 | −112.1 | AII125-8 GGC55/JPC56 | 818 | BF | Keigwin (2002) |
| 23.6 | −111.6 | MV99-MC17/GC32/PC10 | 430 | BF | Lindsay et al. (2016) |
| 23.5 | −111.6 | MV99-MC19/GC31/PC08 | 705 | BF | Marchitto et al. (2007) |
| 23.2 | −111.1 | MV99-GC38 | 1,270 | BF | Lindsay et al. (2016) |
| 20.1 | 117.4 | GIK17940 | 1,727 | BF | Sarnthein et al. (2007); Sarnthein et al. (2015) |
| 19.5 | 116.3 | MD05-2904 | 2,066 | BF | Wan and Jian (2014) |
| 18.9 | 115.8 | 50-37KL | 2,695 | BF | Broecker, Peng, et al. (1990) |
| 18.3 | 57.7 | RC27-14 | 596 | BF | Bryan et al. (2010) |
| 18.0 | 57.6 | RC27-23 | 820 | BF | Bryan et al. (2010) |
| 15.4 | −51.1 | Gramberg Seamount deep-sea corals | 1,492–1,544 | DC | Chen et al. (2015) |
| 14.9 | −48.2 | Vayda Seamount deep-sea corals | 795–1,827 | DC | Chen et al. (2015) |
| 11.9 | −78.7 | Vema 28-122 | 1,800 | BF | Broecker, Klas, et al. (1990) |
| 10.7 | −44.6 | Vema Fracture Zone deep-sea corals | 1,097–1,657 | DC | Chen et al. (2015) |
| 9.2 | −21.3 | Carter Seamount deep-sea corals | 973–2,100 | DC | Chen et al. (2015) |
| 8.8 | 111.4 | MD05-2896 | 1,657 | BF | Wan and Jian (2014) |
| 7.2 | 112.1 | V35-05 | 1,953 | BF | Andree et al. (1986); Broecker, Andree, et al. (1988); Broecker, Klas, et al. (1988) |

**Table 1** *(continued)*

| Latitude | Longitude | Sediment core/coral name | Modern water depth (m) | Substrate | References |
|---|---|---|---|---|---|
| 7.2 | 112.2 | V35-06 | 2,030 | BF | Andree et al. (1986) |
| 6.0 | 126.0 | MD98-2181 | 2,100 | BF | Broecker et al. (2004) |
| 5.6 | −26.9 | Knipovich Seamount deep-sea corals | 749–2,814 | DC | Chen et al. (2015) |
| 4.9 | −43.2 | KNR110 50GGC | 3,995 | BF | Broecker, Klas, et al. (1990) |
| 4.6 | −43.4 | KNR110 66GGC | 3,547 | BF | Broecker, Klas, et al. (1990) |
| 4.3 | −43.5 | KNR110 82GGC | 2,816 | BF | Broecker, Klas, et al. (1990) |
| 4.0 | −114.2 | KNR73 6PG | 3,806 | BF | Keigwin and Lehman (2015) |
| 2.3 | −30.6 | GeoB 1503-1 | 2,306 | DC | Mangini et al. (1998) |
| 1.8 | −110.3 | KNR73 4PC | 3,681 | BF | Keigwin and Lehman (2015) |
| 1.0 | 160.5 | V28-238 | 3,120 | BF | Broecker, Klas, et al. (1988) |
| 1.0 | 130.0 | MD01-2386 | 2,800 | BF | Broecker et al. (2008) |
| 0.0 | −86.5 | ME0005-24JC | 2,941 | BF | Keigwin and Lehman (2015) |
| 0.0 | −86.5 | ODP1240 | 2,921 | BF | de la Fuente et al. (2015) |
| −0.4 | −106.2 | KNR73 3PC | 3,606 | BF | Keigwin and Lehman (2015) |
| −1.0 | 146.0 | MD97-2138 | 1,900 | BF | Broecker et al. (2004) |
| −1.2 | −89.7 | VM21-30 | 617 | BF | Stott et al. (2009) |
| −1.3 | −11.9 | RC24-08 | 600 | Deep-Dwelling PF | Cléroux et al. (2011) |
| −1.6 | 162.6 | S67 FFC15 | 4,250 | BF | Keigwin and Lehman (2015) |
| −2.0 | −140.0 | TTN013-18 | 4,400 | BF | Broecker and Clark (2010) |
| −3.3 | −102.5 | PLDS 7G | 3,253 | BF | Keigwin and Lehman (2015) |
| −3.5 | −35.4 | MD09-3256Q | 3,537 | BF | Freeman et al. (2016) |
| −3.6 | −84.0 | TR163-31 | 3,210 | BF | Shackleton et al. (1988) |
| −4.2 | −37.1 | GS07-150-17/1GC-A | 1,000 | BF | Freeman et al. (2015) |
| −4.2 | −36.4 | MD09-3257 | 2,344 | BF | Freeman et al. (2016) |
| −4.5 | −102.0 | VNTR01-10GGC | 3,410 | BF | Keigwin and Lehman (2015) |
| −10.3 | −111.3 | TT154-10 | 3,225 | BF | Broecker, Andree, et al. (1988); Broecker, Klas, et al. (1988) |
| −13.1 | 121.7 | MD01-2378 | 1,783 | BF | Sarnthein et al. (2011) |
| −22.4 | −40.0 | ENG-111 | 621 | DC | Mangini et al. (2010) |
| −24.2 | −43.3 | 21210009 | 781 | DC | Mangini et al. (2010) |
| −27.5 | −46.3 | KNR159-5-78GGC | 1,829 | BF | Lund et al. (2015) |
| −27.5 | −46.5 | KNR159-5-36GGC | 1,268 | BF | Sortor and Lund (2011) |
| −35.3 | 176.6 | S794 | 2,406 | BF | Sikes et al. (2016) |
| −36.2 | −73.7 | SO161-SL22 | 1,000 | BF | De Pol-Holz et al. (2010) |
| −36.7 | 176.6 | RR0503-TC83/JPC83 | 1,627 | BF | Sikes et al. (2016) |
| −37.0 | 176.6 | RR0503-JPC79 | 1,165 | BF | Sikes et al. (2016) |
| −37.0 | 177.2 | H213 | 2,065 | BF | Sikes et al. (2000) |
| −37.2 | 177.7 | H209 | 1,675 | BF | Sikes et al. (2000) |
| −37.4 | 177.0 | RR0503-JPC64 | 651 | BF | Rose et al. (2010) |
| −39.5 | −176.4 | S931 | 4,097 | BF | Sikes et al. (2016) |
| −39.9 | −177.7 | RR0503-JPC41 | 3,836 | BF | Sikes et al. (2016) |
| −39.9 | −176.2 | RR0503-JPC36 | 4,389 | BF | Sikes et al. (2016) |
| −40.4 | 178.0 | MD97-2121 | 2,314 | BF | Skinner et al. (2015) |
| −41.1 | 7.8 | TNO57-21 | 4,981 | BF | Barker et al. (2010) |
| −43.5 | 174.9 | MD97-2120 | 1,210 | BF | Rose et al. (2010) |
| −44.1 | −14.2 | MD07-3076 | 3,770 | BF | Skinner et al. (2010); Gottschalk et al. (2016) |
| −44.8 | 174.5 | PS75/104-1 | 835 | BF | Ronge et al. (2016) |
| −45.0 | 148.0 | Tasmania deep-sea corals | 1,428–1,947 | DC | Hines et al. (2015) |
| −45.1 | 174.6 | SO213-84-1 | 972 | BF | Ronge et al. (2016) |
| −45.1 | 179.5 | U938 | 2,700 | BF | Sikes et al. (2000) |
| −45.8 | 177.1 | SO213-84-1 | 2,498 | BF | Ronge et al. (2016) |
| −45.8 | 176.6 | SO213-82-1 | 2,066 | BF | Ronge et al. (2016) |
| −45.8 | 179.6 | SO213-79-2 | 3,140 | BF | Ronge et al. (2016) |
| −46.0 | −75.0 | MD07-3088 | 1,536 | BF | Siani et al. (2013) |
| −46.2 | −178.0 | SO213-76-2 | 4,339 | BF | Ronge et al. (2016) |
| −54.2 | −125.4 | PS75/059-2 | 3,613 | BF | Ronge et al. (2016) |
| −54.5 | −62.2 | Burdwood Bank deep-sea corals1 | 318 | DC | Burke and Robinson (2012) |

**Table 1** *(continued)*

| Latitude | Longitude | Sediment core/coral name | Modern water depth (m) | Substrate | References |
|---|---|---|---|---|---|
| −55.0 | −62.0 | Burdwood Bank deep-sea corals2 | 816–1,516 | DC | Burke and Robinson (2012); Chen et al. (2015) |
| −59.4 | −68.5 | 47396 | 1,125 | DC | Robinson and van de Flierdt (2009) |
| −59.7 | −68.7 | 47396B | 1,125 | DC | Goldstein et al. (2001) |
| −60.0 | −69.0 | Sars Seamount deep-sea corals | 695–1,750 | DC | Burke and Robinson (2012); Chen et al. (2015) |
| −60 | −58 | Shackleton Fracture Zone deep-sea corals | 806–823 | DC | Burke and Robinson (2012); Chen et al. (2015) |
| −61.0 | −66.0 | Interim seamount deep-sea corals | 983–1,196 | DC | Burke and Robinson (2012); Chen et al. (2015) |

of the samples considered in this study come from the literature (Table 1), with one notable exception: for the samples whose calendar age is determined from radiocarbon dating, we recalibrate all radiocarbon ages to calendar ages with the most recent relationship of IntCal13 (Reimer et al., 2013), if this was not done in the original publications. For this calculation, we use the surface reservoir ages from the publications (Table 1). Note that about 71% of the compiled radiocarbon data fall within the time interval from 10 to 20 kyr B.P. (Figure 2), which is the interval of interest in this study. Note also that all data in our compilation have been recalculated to be consistent with the revised estimate of the $^{14}C$ half-life (Audi et al., 2003).

### 2.1.1. Estimation of $\Delta^{14}C$ Values Within Ocean Volumes

We partition the compiled deep water $\Delta^{14}C$ data into 10 different oceanic volumes corresponding to the 10 intermediate and deep boxes of the model used for this study (Figure 1 and section 2.2). The global sea level during the LGM is estimated to have been about 130 m lower than today (Clark et al., 2009; Lambeck et al., 2014), which implies that the depths of the glacial and deglacial samples should have been shallower than today by 130 m or less. However, the deglacial changes in global sea level have only a minor effect on the repartition of the samples among the intermediate and deep ocean boxes (Figure S1). As a result, the modern depths of the samples are used. Data from the Arctic Ocean and the Nordic Seas are not included in our study, for these regions are not covered by the 10 subsurface boxes of the model (section 2.2).

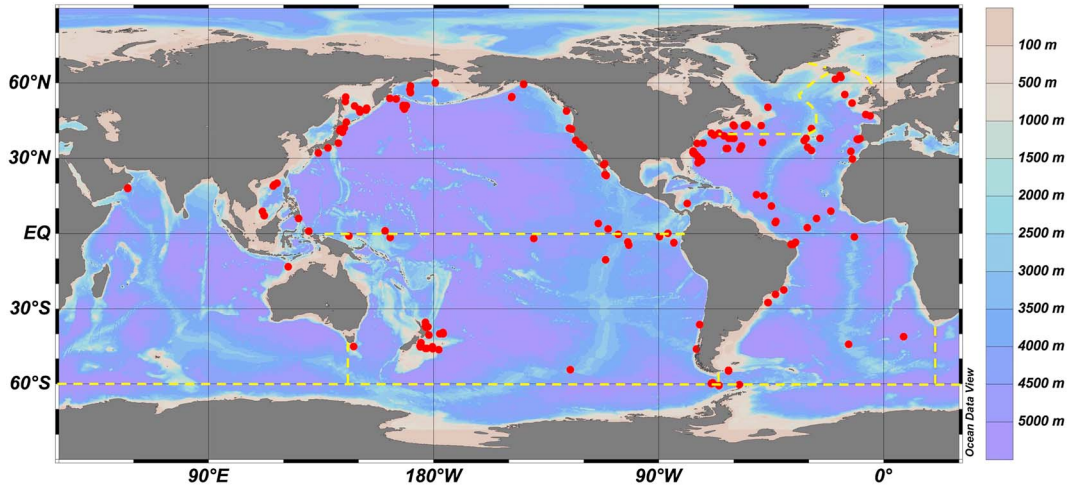


**Figure 1.** Locations of coring and dredging sites where samples have been collected to estimate deep water $\Delta^{14}C$ according to our compilation (red dots). Yellow dashed lines delineate the lateral boundaries of the intermediate and deep boxes of the model (CYCLOPS). The interface between the Circumpolar Deep Water box and the intermediate and deep boxes in the Atlantic, Pacific, and Indian Oceans is sloping down northward, which is not rendered in the figure (only the southernmost latitude of the interface is shown).

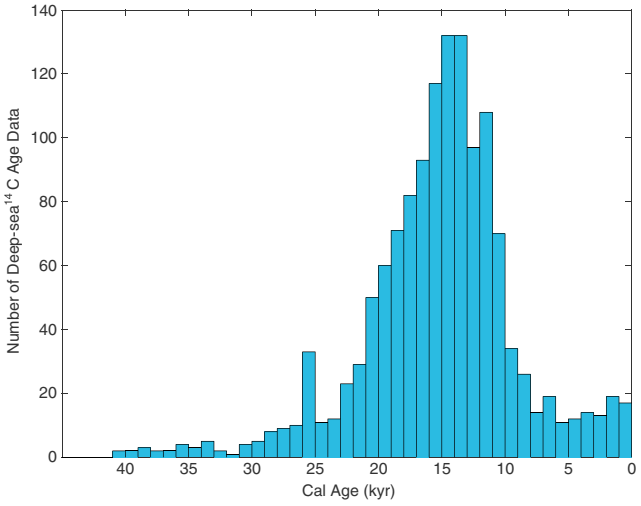


**Figure 2.** Distribution of the calendar ages of the published and new deep-sea $^{14}$C age data compiled in this study.

To increase the robustness of $\Delta^{14}$C estimates for the model boxes, estimates of deep water $\Delta^{14}$C in each box are averaged in temporal bins. The bins are adjacent, have uniform duration (see below), and span together the interval from 10 to 20 kyr B.P. In order to prevent single-core $\Delta^{14}$C values from dominating our results, bins containing deep water $\Delta^{14}$C estimates originating from only one record are excluded from our analysis.

The width (duration) of the bins is selected on the basis of the uncertainties in the calendar ages of the compiled data (Figure 3). The median error (two standard deviations) of the calendar ages between 10 and 20 kyr B.P. amounts to ~ 300 years. This value is probably a lower estimate due to some factors that were not considered in the original publications, such as sedimentation rate changes between chronological tie points (interpolation errors), reservoir age changes, and open-system behavior for deep-dwelling corals. Nevertheless, based on this value, a bin width of 600 years is chosen for the calculation of deep water $\Delta^{14}$C values, unless stipulated otherwise. For the bin duration of 600 years, the $\Delta^{14}$C estimates are averaged in the bins [20.1–19.5] kyr B.P., [19.5–18.9] kyr B.P., …, [10.5–9.9] kyr B.P. The bin $\Delta^{14}$C values are defined at the center of the bins and occur at the same times for all boxes, for example, the $\Delta^{14}$C values for the bin [15.3–14.7] kyr B.P. are all defined at 15.0 kyr B.P. The effect of bin width is discussed in section 4.1.

#### 2.1.2. Estimation of Time-Average Binned $\Delta^{14}$C Errors

The bin $\Delta^{14}$C values have various sources of uncertainty arising from (i) errors in the original $\Delta^{14}$C data (e.g., instrumental and chronological errors), (ii) the assumption that site-specific data reflect basin-scale averages, and (iii) temporal variability of deep water $\Delta^{14}$C within a bin.

In our analysis, the error in a bin $\Delta^{14}$C value is set equal to $\sqrt{\sigma_a^2 + \sigma_b^2}$, where $\sigma_a$ is the standard error of the mean of deep water $\Delta^{14}$C data falling in that bin and $\sigma_b$ is the mean of the $\Delta^{14}$C errors in that bin calculated from published analytical and calendar age uncertainties (for samples whose calendar age uncertainty is not reported, a value of 300 years is used based on the bin width). This approach has the benefit of accounting for not only the error from the data themselves but also for the spatial (e.g., intercore) variability and temporal (e.g., intracore) variability. The temporal mean of the bin $\Delta^{14}$C errors estimated using our method varies from 29‰ to 53‰, depending on the box.

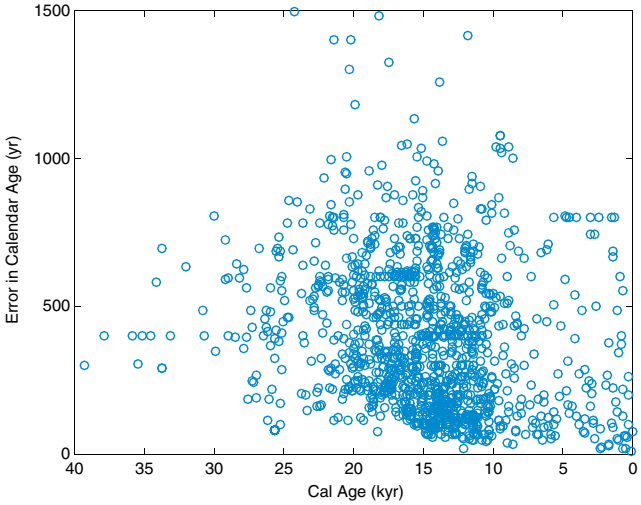


**Figure 3.** Published errors (two standard deviations) in the calendar ages of the deep-sea $^{14}$C age data compiled in this study. The median error for the time interval between 10 and 20 kyr B.P. amounts to ~ 300 years.

### 2.2. Box Model

The model used in this study is a 16-box model of the world oceans (excluding the Arctic Ocean), called CYCLOPS. This model was initially developed by Keir (1988), has been the subject of different extensions (e.g., Hain et al., 2010; Sigman et al., 1998), and has been applied in a variety of paleoceanographic studies (for recent works see, e.g., Galbraith et al., 2015; Hain et al., 2011, 2014b). It includes 6 surface boxes, and 10 intermediate and deep boxes (Figure 4). The lateral boundaries of the surface boxes coincide with latitude and longitude lines, except in the North Atlantic (Keir, 1988). Lateral boundaries of subsurface boxes are not everywhere the same as those of surface boxes (Figure 1): whereas the zonal boundaries of Southern Hemisphere surface boxes are latitude lines, the interfaces between the Circumpolar Deep Water box and the intermediate and deep boxes in the Atlantic, Indian, and Pacific Oceans are sloping in the meridional direction in order to reflect the southward uplift of density surfaces in the Southern Ocean (Keir, 1988).

The volume transports in the box model (Figure 4) were estimated from measurements of a variety of tracers in the modern ocean, including

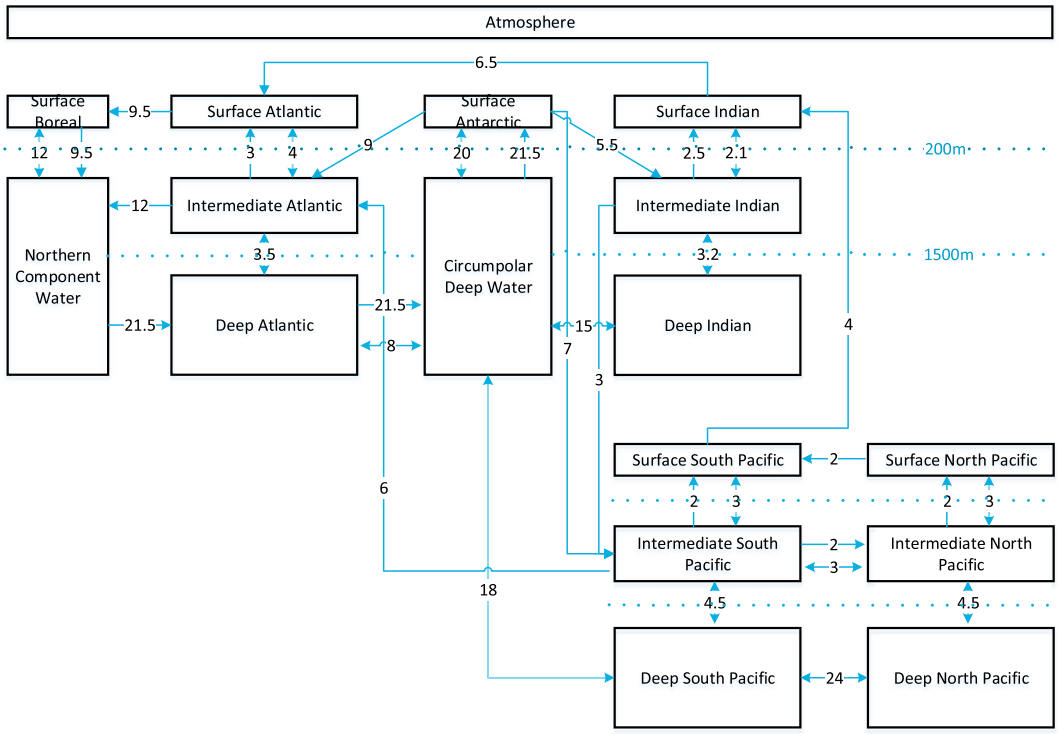


**Figure 4.** Schematic diagram of the box model CYCLOPS (after Keir, 1988; Sigman et al., 1998). The numbers in black indicate the volume fluxes between the boxes in units of Sv (1 Sv = $10^6$ $m^3$ $s^{-1}$).

dissolved phosphorous, dissolved oxygen, dissolved inorganic carbon (DIC), alkalinity, and the $^{13}C/^{12}C$ ratio and $\Delta^{14}C$ of DIC (Keir, 1988). They depict conventional features of the modern circulation, such as the formation of deep waters in the northern North Atlantic (at a rate of 9.5 sverdrup (Sv), where 1 Sv = $10^6$ $m^3$ $s^{-1}$), the upwelling in the Southern Ocean (21.5 Sv), and the transports of waters to the rest of the ocean (Figure 4). The model analogue of the Atlantic meridional overturning circulation amounts to 21.5 Sv, broadly consistent with more recent observational estimates (e.g., Lumpkin & Speer, 2003, 2007; Lumpkin et al., 2008; Rayner et al., 2011).

### 2.2.1. Definition of Radiocarbon Concentration

The radiocarbon concentrations in the model are defined as follows. Consider the conventional definition of $\Delta^{14}C$,

$$\Delta^{14}C = \left(\mathrm{Fm}\times e^{\frac{\text{cal age}}{8{,}223}} - 1\right)\times 1{,}000‰. \quad (1)$$

Here Fm is the "fraction modern" reported from the instrument, that is, the $^{14}C/^{12}C$ ratio (normalized to $\delta^{13}C$ of −25‰) of the sample divided by that of a standard (McNichol et al., 2001), "cal age" is the calendar age of the sample, and the mean life of 8,223 years is based on the 5,700 year half-life (Audi et al., 2003). From (1), we define the radiocarbon concentrations in the model as

$$C = \frac{\Delta^{14}C}{1{,}000} + 1 = \mathrm{Fm}\times e^{\frac{\text{cal age}}{8{,}223}}. \quad (2)$$

Thus, $C$ (dimensionless) represents the $^{14}C/^{12}C$ ratio of the sample when the carbonate was formed, normalized to that of the standard. For example, a $\Delta^{14}C$ value of −200‰, such as observed in the modern deep Pacific (e.g., Broecker & Peng, 1982), would correspond to a radiocarbon concentration $C$ = 0.8, whereas a $\Delta^{14}C$ value of −1,000‰ (equivalent to infinite calendar age) would correspond to $C$ = 0.

Notice that radiocarbon concentration, instead of $^{14}C$ age, is used in our analysis, because $^{14}C$ concentration as represented by $\Delta^{14}C$ is a straightforward variable to implement in a tracer transport model, in contrast to age-related concepts. On the other hand, time series of $\Delta^{14}C$ do not place changes in deep ocean $^{14}C$ content

in the context of atmospheric changes. For this reason, in this paper, the variations in deep water $\Delta^{14}C$ are illustrated jointly with those of atmospheric $\Delta^{14}C$ as reconstructed by IntCal13.

#### 2.2.2. Governing Equation for Radiocarbon

The radiocarbon concentration in each deep and intermediate box of the model evolves according to the governing equation:

$$\frac{dC_i}{dt} = \frac{1}{V_i}\sum_{j\neq i} J_{ji}C_j - \frac{C_i}{V_i}\sum_{j\neq i} J_{ij} - \lambda C_i. \quad (3)$$

Here $C_i$ is the radiocarbon concentration in box $i$, $V_i$ is the volume of box $i$, $J_{ji}$ is the volume transport from box $j$ to box $i$, and $\lambda$ = (1/8,223) year$^{-1}$ is the $^{14}C$ radioactive decay constant. Thus, $C_i$ is the concentration in an intermediate or deep box, and $C_j$ is the concentration in an intermediate, deep, or surface box. Although $C_i$ is a concentration ratio, its governing equation can be cast in the form of a governing equation for a concentration with at least first-order accuracy (Fiadeiro, 1982). On the right-hand side of (3), the first term represents the supply of $^{14}C$ due to water transport from the surrounding boxes, the second describes the removal of $^{14}C$ from water export to the surrounding boxes, and the last is the rate of disappearance of $^{14}C$ due to radioactive decay within the box. Since our study aims to evaluate the (in)consistency of the paleodata with modern ventilation rates, the volume transports ($J_{ij}$) are fixed to their modern values (Figure 4). Other effects such as due to organic matter remineralization and carbonate dissolution (negligible at least to first order; Fiadeiro, 1982), hydrothermal processes, and water-sediment fluxes are neglected. The omission of the effect of organic C remineralization (the major biological carbon flux from the surface to deep ocean (Hain et al., 2014a)) is further motivated by a previous study showing that changes in this effect have a minor influence on the oceanic $\Delta^{14}C$ distributions simulated in experiments of ocean circulation change with a zonally averaged circulation-biogeochemistry model (maximum difference ranging from −9‰ to 7‰, depending on the oceanic basin and the experiment; Marchal et al., 1999). Details about the model used in this study are reported in Text S1.

### 2.3. Inverse Method

#### 2.3.1. Statement of the Problem

The box model described in section 2.2 is fit to the deep water $\Delta^{14}C$ data summarized in section 2.1 (for details see Text S1). Briefly, we use an inverse method that relies on a whole-domain approach (e.g., Amrhein et al., 2015; Wunsch, 2006). In this approach, the finite difference forms of the radiocarbon governing equation (3) for the different subsurface boxes and different time steps, with the unsteady term $dC_i/dt$ retained, are combined so as to reduce the fitting problem to the solution of a set of linear algebraic equations (equation (4) below). The model fit to the data is achieved by adjusting the $\Delta^{14}C$ values in the surface boxes of the model. These values are obtained by solving a system of linear algebraic equations,

$$\delta\bar{\mathbf{y}} = \bar{\mathbf{G}}\bar{\mathbf{c}}_s + \bar{\mathbf{n}}. \quad (4)$$

Here $\delta\bar{\mathbf{y}}$ is a vector of the deep water $^{14}C$ concentration data binned in space and time and expressed as anomalies from the initial time step (Text S1), $\bar{\mathbf{G}}$ is a matrix that represents the effect of ocean circulation, $\bar{\mathbf{c}}_s$ is a vector including the surface water $^{14}C$ concentrations, and $\bar{\mathbf{n}}$ is a vector including the errors of the data in $\delta\bar{\mathbf{y}}$. The system (4) includes one equation for each subsurface box and for each bin for which a deep water $\Delta^{14}C$ estimate is available. It provides a formal statement of the inverse problem: the inference of surface water $^{14}C$ concentrations ($\bar{\mathbf{c}}_s$) from deep water $^{14}C$ concentration data ($\delta\bar{\mathbf{y}}$) under modern circulation conditions ($\bar{\mathbf{G}}$) and in the presence of observational errors ($\bar{\mathbf{n}}$). In other words, time series of surface water $^{14}C$ concentrations are inferred from a fit of the box model of modern ocean ventilation to the deep water $\Delta^{14}C$ data records, given the presence of errors in the data.

#### 2.3.2. Method of Solution

Time series of $^{14}C$ concentration in each surface box are inferred using a three-step approach. First, each equation in (4) is divided by the error in the corresponding bin $\Delta^{14}C$ in order to give more weight to the bin $\Delta^{14}C$ values with smaller uncertainties (row scaling; Wunsch, 2006). Each quantity in (4) affected by row scaling is referred below to with an asterisk; for example, the scaled vector $\delta\bar{\mathbf{y}}$ is referred to as $\delta\bar{\mathbf{y}}_*$. Second, a first guess of the solution, $\bar{\mathbf{c}}_{s0}$, is obtained from (i) the atmospheric $\Delta^{14}C$ reconstruction (Reimer et al., 2013), (ii) observational estimates of modern (preindustrial) reservoir ages for the six surface boxes

(Bard, 1988), and (iii) the effect of atmospheric $pCO_2$ on sea surface reservoir age (Galbraith et al., 2015). Specifically, modern reservoir age is set equal to 1,000 years for the Antarctic box and 400 years for the other surface boxes, which values are consistent with observational estimates reported by Bard (1988), and the reservoir age is set to increase with decreasing atmospheric $pCO_2$ (Galbraith et al., 2015), yielding an offset of ~ 250 years from today at the LGM. Finally, the solution $\overline{\boldsymbol{c}}_s$ is expressed as the sum of the first guess and a deviation, that is, $\overline{\boldsymbol{c}}_s = \overline{\boldsymbol{c}}_{s0} + \overline{\boldsymbol{c}}_s'$. The deviation $\overline{\boldsymbol{c}}_s'$ is obtained from the solution of a new set of equations (for a similar approach, see Gebbie, 2012),

$$\delta\overline{\boldsymbol{y}}_*' = \overline{\boldsymbol{G}}_*\overline{\boldsymbol{c}}_s' + \overline{\boldsymbol{n}}_*, \tag{5}$$

where $\delta\overline{\boldsymbol{y}}_*' = \delta\overline{\boldsymbol{y}}_* - \overline{\boldsymbol{G}}_*\overline{\boldsymbol{c}}_{s0}$. Thus, we are solving for deviations of $^{14}C$ concentration in each surface box from a hypothetical value based on atmospheric $\Delta^{14}C$ and $pCO_2$ changes and modern (preindustrial) reservoir ages.

The system (5) is solved for $\overline{\boldsymbol{c}}_s'$ using singular value decomposition, SVD (e.g., Wunsch, 2006). To this end, the coefficient matrix $\overline{\boldsymbol{G}}_*$ is decomposed as

$$\overline{\boldsymbol{G}}_* = \boldsymbol{U}\boldsymbol{\Lambda}\boldsymbol{V}^T, \tag{6}$$

where $\boldsymbol{U}$ ($\boldsymbol{V}$) is an orthonormal matrix containing the left (right) singular vectors of $\overline{\boldsymbol{G}}_*$ and $\boldsymbol{\Lambda}$ is a nonsquare diagonal matrix with the singular values of $\overline{\boldsymbol{G}}_*$ ranked in order of decreasing magnitude along the diagonal. The SVD solution of (5) is

$$\widehat{\overline{\boldsymbol{c}}}_s' = \sum_{i=1}^{K} \frac{\boldsymbol{u}_i^T \delta\overline{\boldsymbol{y}}_*'}{\lambda_i}\boldsymbol{v}_i + \sum_{i=K+1}^{N} \alpha_i \boldsymbol{v}_i, \tag{7}$$

where $\boldsymbol{u}_i$ and $\boldsymbol{v}_i$ are singular vectors (the $i$th column of $\boldsymbol{U}$ and $\boldsymbol{V}$, respectively), $\lambda_i$ is a singular value (the $i$th element along the diagonal of $\boldsymbol{\Lambda}$), $K$ is the number of singular values different from zero, and $\alpha_i$ is an unknown expansion coefficient. On the right-hand side of (7), the first term represents the contribution due to structures in $\overline{\boldsymbol{c}}_s'$ that can be determined from the data (the range of $\overline{\boldsymbol{G}}_*$) and the second term represents the contribution due to structures that cannot be determined from the data (the null-space of $\overline{\boldsymbol{G}}_*$). It can be shown that the SVD solution (7) is a weighted least squares solution when this exists, that is, in the absence of a null-space for which $K = N$ (e.g., Wunsch, 2006). The "particular SVD solution" includes only the first term and is biased for $K < N$.

The error covariance matrix, or uncertainty, of the SVD solution $\widehat{\overline{\boldsymbol{c}}}_s'$ is

$$\boldsymbol{P}_{\widehat{\overline{\boldsymbol{c}}}_s'} = \sum_{i=1}^{K}\sum_{j=1}^{K} \boldsymbol{v}_i \frac{\boldsymbol{u}_i^T \langle \overline{\boldsymbol{n}}_* \overline{\boldsymbol{n}}_*^T \rangle \boldsymbol{u}_j}{\lambda_i \lambda_j} \boldsymbol{v}_j^T + \sum_{i=K+1}^{N}\sum_{j=K+1}^{N} \boldsymbol{v}_i \langle \alpha_i \alpha_j \rangle \boldsymbol{v}_j^T, \tag{8}$$

where $\langle \overline{\boldsymbol{n}}_* \overline{\boldsymbol{n}}_*^T \rangle$ is the error covariance matrix for the observational estimates of $^{14}C$ concentration in $\delta\overline{\boldsymbol{y}}_*'$ and $\langle\cdot\rangle$ denotes the expected value. The diagonal elements of $\langle \overline{\boldsymbol{n}}_* \overline{\boldsymbol{n}}_*^T \rangle$ are equal to 1 (since equation (4) has been scaled) and the off-diagonal elements of $\langle \overline{\boldsymbol{n}}_* \overline{\boldsymbol{n}}_*^T \rangle$ are set equal to zero, assuming negligible error covariances; that is, $\langle \overline{\boldsymbol{n}}_* \overline{\boldsymbol{n}}_*^T \rangle$ is an identity matrix. The first term on the right-hand side of (8) represents the contribution due to the observational errors, whereas the second is the contribution due to presence of a null-space in the solution (if any). Since the expansion coefficients $\alpha_i$ ($i = K + 1, \ldots, N$) are unknown, the second term in (8) is sometimes set to zero. In this case, the uncertainties in the elements of the solution ($\widehat{\overline{\boldsymbol{c}}}_s'$) should be viewed as lower estimates.

## 3. Results

In this section, we first describe our compilation of deep ocean $\Delta^{14}C$ data for the past 40 kyr. The box model of modern ocean ventilation is then fit to the deep ocean $\Delta^{14}C$ data (bin values) by allowing $\Delta^{14}C$ to vary in the model surface boxes.

### 3.1. Synthesis of Deep Water $\Delta^{14}C$ Data

The compiled $\Delta^{14}C$ data attributed to different intermediate and deep oceanic volumes are shown in Figure 5. As expected, the oceanic $\Delta^{14}C$ values are lower than the reconstructed $\Delta^{14}C$ in the contemporaneous atmosphere, with a few exceptions presumably due to chronological errors.

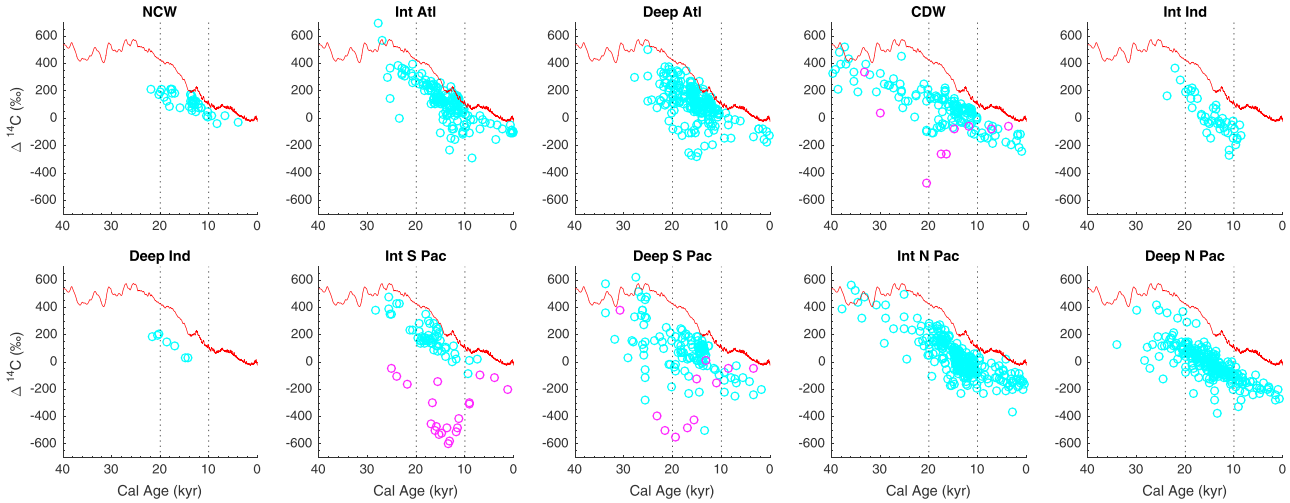


**Figure 5.** Compiled deep water $\Delta^{14}C$ data for the 10 intermediate and deep boxes of the model (cyan circles). Magenta circles show data potentially influenced by hydrothermal processes (Ronge et al., 2016; Stott et al., 2009). The atmospheric $\Delta^{14}C$ reconstruction is shown in red for reference (Reimer et al., 2013). Vertical dotted lines delineate the time interval 10–20 kyr B.P. The order in which the different panels appear is arbitrary, although it is intended to broadly correspond to the sense of the estimated movement of deep waters from the northern North Atlantic (leftmost top panel) to the deep North Pacific in the modern ocean (rightmost bottom panel).

Particularly large variations in deep water $\Delta^{14}C$ are observed in the Intermediate South Pacific, the Deep South Pacific, and the Circumpolar Deep Water boxes (magenta circles in Figure 5). The $\Delta^{14}C$ record from 617 m water depth near the Galapagos Archipelago (Stott et al., 2009) shows very low values compared to other $\Delta^{14}C$ records for the Intermediate South Pacific. These very low values have been suggested to reflect a supply of old carbon from hydrothermal activity (e.g., Lund & Asimow, 2011; Stott & Timmermann, 2011). Likewise, two records close to plate boundaries in the South Pacific (in the Deep South Pacific and Circumpolar Deep Water boxes of the model) display very low $\Delta^{14}C$ values during the LGM and early deglaciation which have been suggested to reflect hydrothermal processes (Ronge et al., 2016). In this section, we exclude the three foregoing records since the model does not include the effect of hydrothermalism; the influence of these records on the model fit to the data is documented in section 4.2.

The most conspicuous feature in the assembled deep water $\Delta^{14}C$ data (Figure 5) is a long-term decrease from about 25 kyr B.P. to the present, similar to the decrease in reconstructed atmospheric $\Delta^{14}C$ over the same time interval (Reimer et al., 2013). In order to quantify the apparent decrease in the assembled data set, we use the rank correlation coefficient Kendall tau (Kendall & Gibbons, 1990). Kendall tau measures the amount of monotonic relationship between two random variables (in the present case, deep water $\Delta^{14}C$ and time), making weaker assumptions about their underlying distributions than more conventional measures of correlation, such as the Pearson correlation coefficient. We find that Kendall tau is negative with $p < 0.05$ in all oceanic basins (Table 2), indicating that the apparent decrease in deep water $\Delta^{14}C$ is significant and ubiquitous in our compilation.

The mean of deep water $\Delta^{14}C$ in the different oceanic regions and in different climatic intervals is calculated to reveal possible spatiotemporal patterns of deep ocean $\Delta^{14}C$ over the deglaciation (Table 3). The climatic intervals include the LGM (defined here as 24–17.6 kyr B.P.), the HS1 (17.6–14.65 kyr B.P.), the Bølling-

**Table 2**
*Kendall Tau Coefficient and Its p Value for the Relationship Between Deep Ocean $\Delta^{14}C$ and Calendar Age (25–0 kyr B.P.)*

| Box | NCW | Int Atl | Deep Atl | CDW | Int Ind | Deep Ind | Int S Pac | Deep S Pac | Int N Pac | Deep N Pac |
|---|---|---|---|---|---|---|---|---|---|---|
| Kendall tau | −0.63 | −0.61 | −0.45 | −0.48 | −0.65 | −0.68 | −0.49 | −0.32 | −0.59 | −0.65 |
| *p* value | <0.01 | <0.01 | <0.01 | <0.01 | <0.01 | 0.04 | <0.01 | <0.01 | <0.01 | <0.01 |

*Note.* A negative value indicates a decrease of deep ocean $\Delta^{14}C$ with time.

**Table 3**
*Mean ± One Standard Error of the Mean of $\Delta^{14}C$ Data for Different Climatic Intervals[a] and Different Subsurface Boxes*

| Box | NCW | Int Atl | Deep Atl | CDW | Int Ind | Deep Ind | Int S Pac | Deep S Pac | Int N Pac | Deep N Pac |
|---|---|---|---|---|---|---|---|---|---|---|
| LGM | 178 ± 14 (10) | 287 ± 17 (23) | 198 ± 15 (61) | 81 ± 26 (22) | 206 ± 25 (10) | 187 ± 13 (4) | 211 ± 20 (16) | 102 ± 20 (27) | 167 ± 16 (34) | 93 ± 13 (59) |
| HS1 | 159 ± 43 (3) | 162 ± 11 (38) | 115 ± 15 (75) | 85 ± 16 (27) | 1 ± 25 (8) | 75 ± 46 (2) | 179 ± 14 (23) | 68 ± 25 (20) | 91 ± 14 (53) | 14 ± 10 (45) |
| BA | 119 ± 9 (14) | 75 ± 19 (24) | 93 ± 15 (30) | 42 ± 10 (19) | 8 ± 20 (9) | NA (1) | 83 ± 20 (3) | 51 ± 21 (33) | 0 ± 9 (51) | −52 ± 12 (47) |
| YD | 86 ± 14 (5) | 71 ± 21 (23) | 59 ± 13 (35) | 53 ± 14 (8) | −50 ± 20 (4) | NA (0) | 50 ± 26 (4) | 70 ± 49 (3) | −43 ± 14 (26) | −67 ± 7 (14) |
| EH | 22 ± 16 (6) | 26 ± 17 (32) | 10 ± 16 (16) | −27 ± 17 (20) | −124 ± 22 (13) | NA (0) | −38 ± 48 (2) | −105 ± 23 (7) | −50 ± 9 (47) | −109 ± 9 (47) |
| LH | NA (1) | −92 ± 9 (11) | −114 ± 14 (8) | −168 ± 19 (7) | NA (0) | NA (0) | NA (0) | −224 ± 20 (2) | −156 ± 13 (21) | −214 ± 13 (9) |
| MODERN[b] | −74 | −87 | −112 | −151 | −111 | −183 | −107 | −188 | −142 | −218 |

*Note.* The number of data in each interval is between parentheses.
[a]The dates for the onset of the BA, the onset of the YD, and the termination of the YD are from Rasmussen et al. (2006) (their Table 4). The date for the onset of HS1 is based on an interpretation by de la Fuente et al. (2015) of Greenland ice core $[Ca^{2+}]$ records compiled in Rasmussen et al. (2008). [b]Mean of water column $\Delta^{14}C$ data corrected for bomb $^{14}C$ (GLODAP; Key et al., 2004).

Allerød (BA, 14.65–12.85 kyr B.P.), the YD (12.85–11.65 kyr B.P.), the early Holocene (EH, 11.65–8 kyr B.P.), and the late Holocene (LH, 4–0 kyr B.P.). Importantly, the LH values agree within two standard errors with basin-scale averages in the modern ocean based on water column $\Delta^{14}C$ measurements corrected for bomb-$^{14}C$ (data synthesis of Key et al., 2004; Table 3 and Figure 6). The agreement supports our working assumption that averages of $\Delta^{14}C$ of fossil carbonates from a few sites can constrain $\Delta^{14}C$ of large oceanic volumes. The $\Delta^{14}C$ decrease from the LGM to the EH would have ranged from 110‰ to 330‰, depending on the oceanic region (Table 3). Interestingly, some spatial patterns seem to have been maintained over time. For example, the $\Delta^{14}C$ of the deep Atlantic appears to have remained higher than that of the deep North Pacific by 100 ± 18‰ to 145 ± 19‰, depending on the climatic interval. For reference, the prebomb $\Delta^{14}C$ averages in these two regions differ by 106‰ according to the data synthesis of Key et al. (2004) (Table 3).

In order to present the evolution of deep water radiocarbon in the context of atmospheric $\Delta^{14}C$ changes, we show the averaged ventilation ages of different records for each box (Figure 7). Here ventilation age is simply defined as the $^{14}C$ age difference between seawater and the contemporaneous atmosphere. A number of features emerge. The mean $^{14}C$ ventilation age for the LGM is often the largest, but the differences with subsequent intervals are not always significant. It is tempting to identify different trends in ventilation age between different basins, although it should be stressed that many of the changes from one time interval to the next are not significant even at the level of one standard error. Nonetheless, some of the changes do seem significant (at the level of two standard errors), such as the reduction in ventilation age from the LGM to the Holocene in the northern North Atlantic (NCW), the Deep Atlantic, the Southern Ocean (CDW), and the Deep North Pacific.

### 3.2. (In)Consistency With Modern Ocean Ventilation

In this section, we test whether the deep water $\Delta^{14}C$ data (bin $\Delta^{14}C$ values) for the time interval from 20 to 10 kyr B.P. can be explained in terms of modern ocean ventilation. First, we examine the extent to which the modern ocean ventilation model can be fitted to the deep water $\Delta^{14}C$ data; the surface $\Delta^{14}C$ values that lead to the fit are considered next.

#### 3.2.1. Evolution of Deep Water $\Delta^{14}C$

The deep water $\Delta^{14}C$ values obtained from the model fit to the data are computed by propagating inferred surface $\Delta^{14}C$ values through the box model, as

$$\delta\widehat{\boldsymbol{y}} = \overline{\boldsymbol{G}}\widehat{\boldsymbol{c}}_s, \tag{9}$$

where $\widehat{\boldsymbol{c}}_s = \overline{\boldsymbol{c}}_{s0} + \widehat{\boldsymbol{c}}'_s$.

The model fit to the data depends on the number $K$ of singular vectors that are retained to construct the solution of the inverse problem (equations (7) and (8)). Among the 96 singular values of the coefficient matrix $\overline{\boldsymbol{G}}_*$, six are numerically vanishing (Figure S2a), suggesting the presence of a solution nullspace (section 2.3.2). A solution obtained from all the singular vectors associated with a nonvanishing $\lambda_i$ ($K = 90$) produces deep water $\Delta^{14}C$ values that overfit the data (Figure 8a); that is, the solution with $K = 90$ includes structures that are not justifiable given the data errors (Text S1).

We therefore consider a model fit obtained with a smaller number of singular vectors ($K = 20$). In this case, we find that the overfit to the deep water $\Delta^{14}C$ data is largely mitigated (Figure 8b). Despite the reduced number of structures allowed in the solution, a good fit to the deep water $\Delta^{14}C$ data is still achieved (Figure 9). In particular, the deep $\Delta^{14}C$ values derived from the fit capture the generally negative trend with time that is suggested both in the original data and in the bin records. Some of these values, mainly in the Intermediate Indian where records come from only one location (Bryan et al., 2010), tend to present systematic differences with the data. However, the model fit to the data overall appears satisfactory, particularly in the light of the data errors (Figure 8b): we find that 87% of the data are fit by the model within two standard deviations (Table 4), a fraction which increases to 91% when residuals from Intermediate Indian are excluded from the calculation.

Differences between the deep water $\Delta^{14}C$ values derived from the fit and the deep water $\Delta^{14}C$ data are worth discussing in more detail (Figure 9). As already mentioned, some of the derived values in the Intermediate Indian tend to systematically deviate from the data, although it should be emphasized

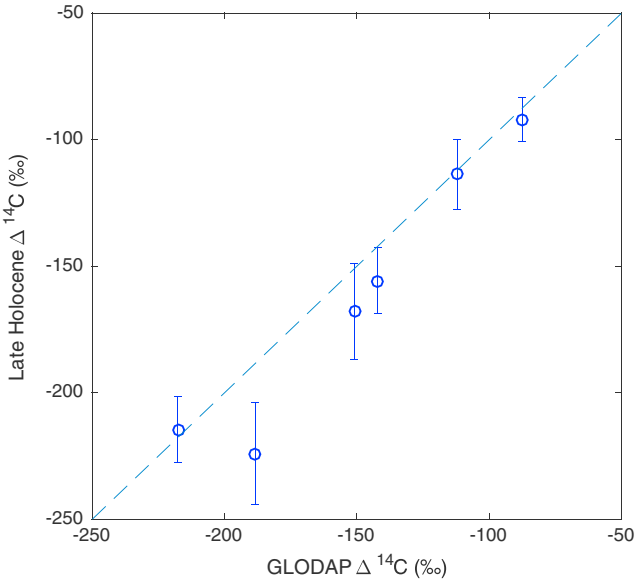


**Figure 6.** Comparison between late Holocene (LH, 0–4 kyr B.P.) $\Delta^{14}C$ derived from seafloor carbonates (vertical axis, mean ± one standard error) and water column $\Delta^{14}C$ corrected for bomb $^{14}C$ derived from GLODAP (horizontal axis; Key et al., 2004). The values displayed are basin-mean averages of Table 3 (from left to right in the figure): Deep N Pac, Deep S Pac, CDW, Int N Pac, Int Ind, and Int Atl. The dashed line is the line of perfect agreement. Notice that the second point (off the diagonal line by more than one standard error) corresponds to the Deep South Pacific, where only two LH data are available (Table 3).

that these data originate from a single location. Perhaps more relevant, deep water $\Delta^{14}C$ values derived from the fit are systematically lower than the observed values in the Intermediate Atlantic, particularly during HS1. A similar offset is suggested in the Intermediate South Pacific during HS1. These results illustrate that the model fit to the whole data set is achieved to the detriment of large and sometimes significant differences with individual data at some locations and during some time intervals. Thus, whereas most of the deep water $\Delta^{14}C$ data can be explained by modern ventilation rates as described in the model, it is also clear that these rates cannot account for all the data. Although consideration of a larger number of structures in the solution ($K > 20$) would reduce the misfits to individual data, such solutions would also tend to overfit the data and thus disregard the data uncertainties, as shown in Text S1.

### 3.2.2. Evolution of Surface Water $\Delta^{14}C$

We find that the surface $\Delta^{14}C$ values inferred from the fit with $K = 20$ are all within the bounds set by the atmospheric and deep ocean observations, in spite of the relatively small error variance of the solution (Figure 10). Notable in the $K = 20$ solution are relatively large deviations of surface water $\Delta^{14}C$ estimated in the boreal Atlantic Ocean and near Antarctica. It thus appears that most of the deep water $\Delta^{14}C$ data could be explained by modern basin-scale circulation, provided that changes in surface water $\Delta^{14}C$ took place at high latitudes. These changes correspond to changes in surface water reservoir age, as indicated by the variable difference between the surface water $\Delta^{14}C$ implied by the fit and the atmospheric $\Delta^{14}C$ reconstructed by IntCal13 (Figure 10). The corresponding reservoir ages increase or decrease with time, depending on the time interval and the surface region (boreal or Antarctic box). However, taking uncertainties into account, most of the surface reservoir age changes are not significant: in the boreal and Antarctic boxes, only 4 over 32 of the surface water $\Delta^{14}C$ values implied by the fit differ from the values expected from the atmospheric $\Delta^{14}C$ and $pCO_2$ records (first guess) by more than two standard deviations (see green stars in Figure 10).

The large (relative to other regions) variations in surface water $\Delta^{14}C$ estimated in the boreal Atlantic and near Antarctica arise from the fact that the deep ocean is mostly ventilated from these regions. Changes in these two regions can be relatively well resolved from deep water data. To demonstrate this, consider the relationship between the actual and estimated time series of surface water $\Delta^{14}C$ values,

$$\mathbf{T}_v \bar{\boldsymbol{c}}_s = \hat{\bar{\boldsymbol{c}}}_s, \tag{10}$$

where $\mathbf{T}_v$ is the solution resolution matrix defined by (e.g., Wunsch, 2006)

$$\mathbf{T}_v = \mathbf{V}_K \mathbf{V}_K^{\mathrm{T}}. \tag{11}$$

Equation (10) shows that each element of the solution, $\hat{\bar{\boldsymbol{c}}}_s$, can be regarded as a linear combination of the actual values in $\bar{\boldsymbol{c}}_s$. Departures of $\hat{\bar{\boldsymbol{c}}}_s$ from $\bar{\boldsymbol{c}}_s$ can thus be investigated from the matrix $\mathbf{T}_v$. One approach for such investigation is to repeatedly calculate $\hat{\bar{\boldsymbol{c}}}_s$ from (10) for a number of vectors $\bar{\boldsymbol{c}}_s$, where each vector has the elements corresponding to a given surface box set to 1 for all times while the elements corresponding to other surface boxes are set to 0 (Amrhein et al., 2015). The elements of $\hat{\bar{\boldsymbol{c}}}_s$ calculated in this way provide a measure of the ability of the deep water $\Delta^{14}C$ data to resolve $\Delta^{14}C$ in the different surface boxes of the model, with a value near 0 indicating poor resolvability and a value near 1 indicating high resolvability.

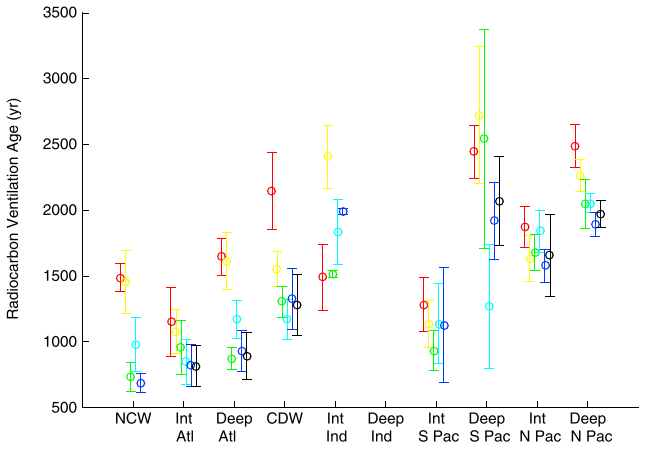


**Figure 7.** Mean ± one standard error of mean radiocarbon ventilation ages for different oceanic volumes and different climatic intervals: LGM (red), HS1 (yellow), BA (green), YD (cyan), EH (blue), and LH (black) (see text).

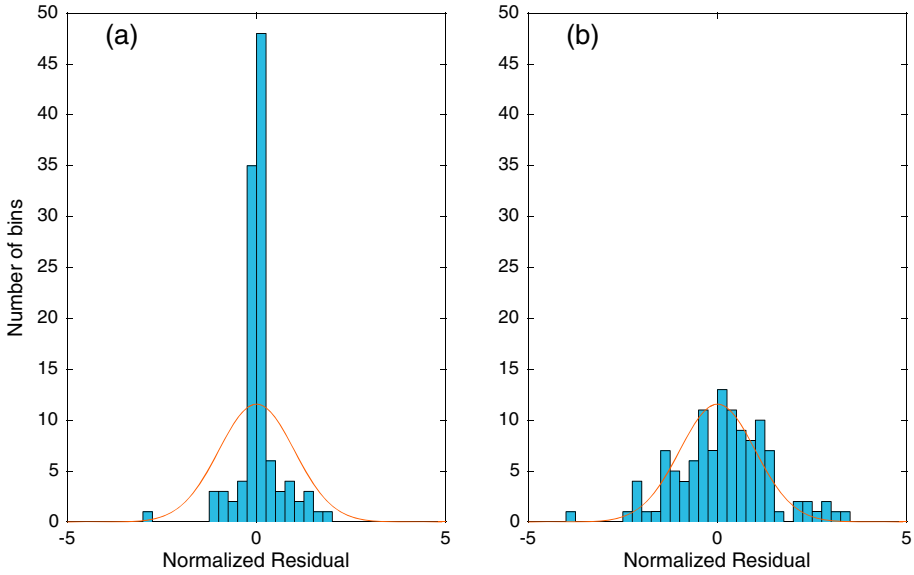


**Figure 8.** Distribution of the difference between fitted and observed (bin) deep water $\Delta^{14}C$ values, normalized to the error in the observed deep water $\Delta^{14}C$, for two different solutions: (a) $K = 90$ and (b) $K = 20$. In each panel, the red curve is the normal (Gaussian) distribution shown for reference.

We find that for $K = 20$, the elements of $\widehat{\bar{\mathbf{c}}}_s$ averaged over the time interval from 20 to 10 kyr B.P. indicate the highest resolvability in the boreal Atlantic and Antarctic boxes (Table 5), which both directly ventilate the deep ocean in the model (Figure 4). The resolvability for the other boxes is close to zero, suggesting that the estimated surface $\Delta^{14}C$ values in those boxes should be interpreted with particular caution. Amrhein et al. (2015) obtained a similar result in an analysis of deglacial benthic $\delta^{18}O$ records using a much more detailed tracer transport model.

## 4. Sensitivity to Data and Model Assumptions

In section 3.2, we have fitted a model of modern ocean ventilation to a compilation of deep water $\Delta^{14}C$ data for the time interval 10–20 kyr B.P. We have found that the residuals of the fit can generally be explained by data errors and that most of the surface water $\Delta^{14}C$ values which produce the fit are oceanographically consistent, in the sense that these values are in general neither significantly larger than atmospheric $\Delta^{14}C$ nor significantly lower than deep sea $\Delta^{14}C$. In this section, we assess the robustness of these results against several assumptions in the analysis. In all cases, model fits to the data obtained with $K = 20$ are considered for a consistent comparison with the solution presented in section 3.2.

### 4.1. Effect of Bin Width

Bin width influences how the deep-sea radiocarbon data are grouped in time within each of the intermediate and deep boxes of the model. It thereby determines the magnitude, uncertainty, and timing of the observational estimates of deep water $\Delta^{14}C$. With a median error of 300 years for the sample calendar ages (Figure 3), a bin width larger than 600 years (the value assumed in section 3.2) does not seem to be generally justified. Here we consider the case where the data are grouped in narrower bins of 400 years.

As expected, the fraction of bins for which deep water $\Delta^{14}C$ data are available decreases in this case: for a bin width of 400 years, about 38% of the bins are empty, compared to 28% for a bin width of 600 years. Consequently, the number of singular values of $\bar{\mathbf{G}}_*$ that are numerically vanishing is larger for a bin width of 400 years (Figure S2b) than for a bin width of 600 years (Figure S2a). Besides, the bin $\Delta^{14}C$ values tend to portray more variability for a bin width of 400 years (Figure S3) than for a bin width of 600 years (Figure 9). This result stems from the fact that for a bin width of 400 years, bin $\Delta^{14}C$ values are derived from a reduced number of data.

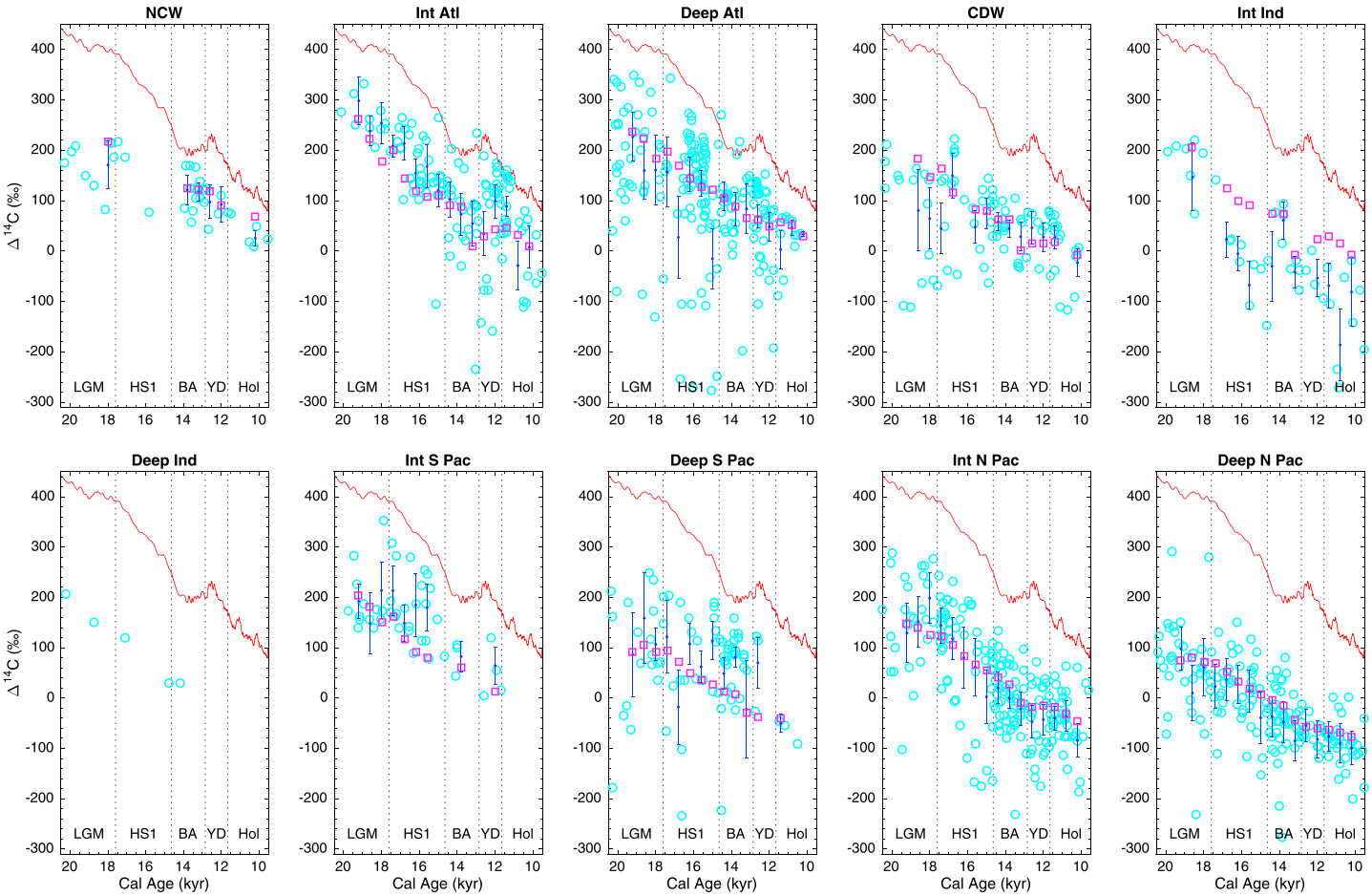


**Figure 9.** Deep water $\Delta^{14}C$ data (cyan circles), deep water bin $\Delta^{14}C \pm$ one standard deviation (dark blue lines), and deep water $\Delta^{14}C$ resulting from the model fit for $K = 20$ (magenta squares). The atmospheric $\Delta^{14}C$ reconstruction (Reimer et al., 2013) is shown for reference (red line). The acronyms at the bottom of each panel refer to different climatic intervals (see text).

We find that the inversion produces similar results to those presented in section 3 (Table 4). The model fit to the deep water $\Delta^{14}C$ data is generally good (Figure S3), with 91% of the data fit within two standard deviations. This fraction is larger than for the case with a bin width of 600 years (87%), because bin errors generally increase with a smaller number of data falling in each bin (larger $\sigma_a$). No values of surface water $\Delta^{14}C$ significantly transgress the bounds set by atmospheric and deep-sea $\Delta^{14}C$ (Figure S4).

### 4.2. Effect of Records With Very Low $\Delta^{14}C$

In this section, we repeat our analysis by adding the three records with particularly low $\Delta^{14}C$ values (Ronge et al., 2016; Stott et al., 2009). The major changes are the appearance of higher-frequency variability in the bin $\Delta^{14}C$ and the presence of larger bin $\Delta^{14}C$ errors in the Intermediate South Pacific, the Deep South Pacific, and the Circumpolar Deep Water boxes (Figure S5). The inverse solution is very similar to that obtained when the three low-$\Delta^{14}C$ records are excluded (Figures S2c, S5, and S6 and Table 4). Thus, data from regions where these records originate appear to have a relatively small influence on the solution.

**Table 4**
*Fraction of Deep Water $\Delta^{14}C$ Data Which Are Not Explained by Modern Ventilation*

| Main solution (section 3) | Bin width 400 year (section 4.1) | Low-$\Delta^{14}C$ records included (section 4.2) | Two horizontal deep Atlantic boxes (section 4.3) | Two vertical deep Atlantic boxes (section 4.4) |
|---|---|---|---|---|
| 13% | 9% | 11% | 13% | 12% |

*Note.* Fraction of data that are not fit to within two standard deviations in the data errors.

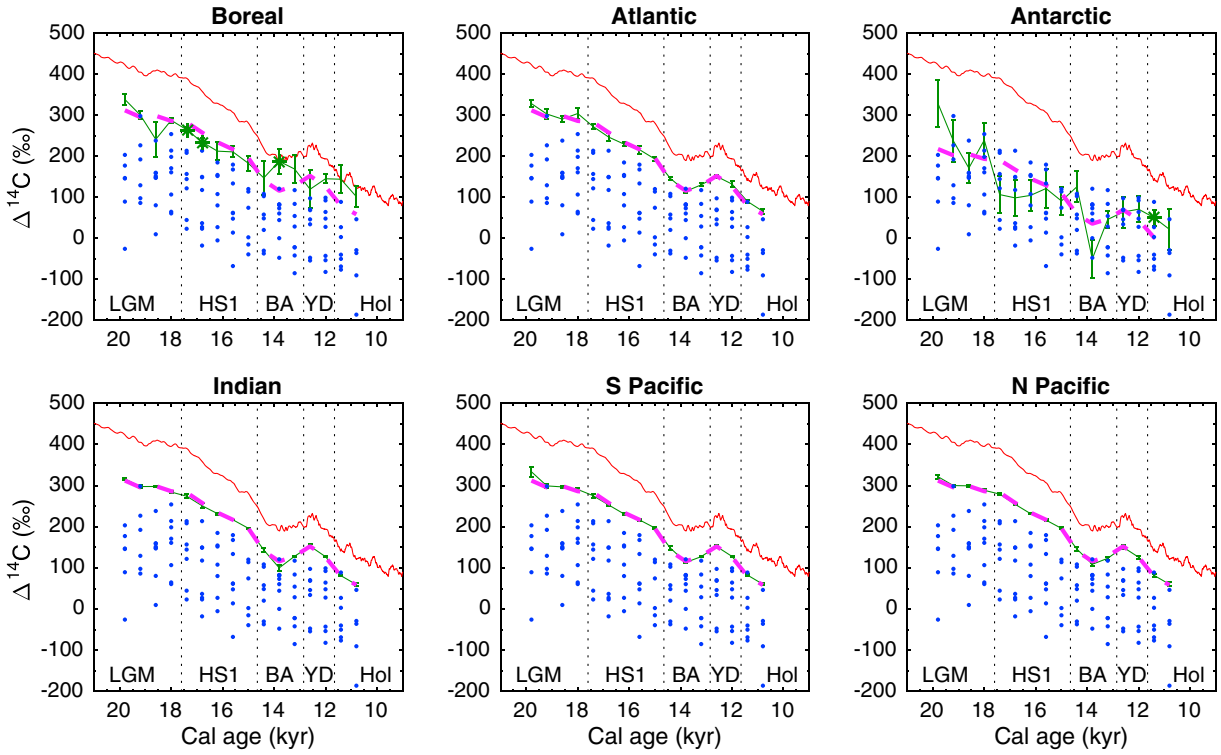


**Figure 10.** Surface water $\Delta^{14}C$ estimated for $K = 20$ (green, with error bar showing ± one standard deviation). The red line is the reconstructed atmospheric $\Delta^{14}C$ (Reimer et al., 2013) and the blue dots are bin $\Delta^{14}C$ values in all the subsurface boxes. Magenta line is the surface water $\Delta^{14}C$ calculated from atmospheric $\Delta^{14}C$ (Reimer et al., 2013) and estimates of preindustrial reservoir ages (Bard, 1988), with the influence of atmospheric $pCO_2$ considered (Galbraith et al., 2015). It is the first guess of the solution as defined in section 2.3.2. The values that differ from this first guess by more than two standard deviations are noted with green stars.

The relative influence on the solution of data from different regions can be illustrated from the data resolution matrix, which is defined as (e.g., Wunsch, 2006)

$$\mathbf{T}_u = \mathbf{U}_K \mathbf{U}_K^{\mathrm{T}}, \tag{12}$$

where $\mathbf{U}_K$ is a matrix containing the first $K$ left singular vectors of $\overline{\mathbf{G}}_*$. The diagonal elements of the matrix $\mathbf{T}_u$ reflect the relative importance of different $\Delta^{14}C$ data (bin values) in determining the surface water $\Delta^{14}C$. These elements are plotted in Figure 11. It is seen that data from the high-latitude North Atlantic boxes are generally more important than those from other regions in determining the solution. The importance of data from the Intermediate South Pacific and Deep South Pacific is relatively small, consistent with the modest effect on the solution of the data originating from these regions.

### 4.3. Effect of Model Architecture: Northern and Southern Deep Atlantic Boxes

Box models such as the one used in this study represent the world oceans with a small number of regions with very large volumes (Figure 1). As a result, and despite the apparent ability of $\Delta^{14}C$ data from a few sites to constrain the volume-averaged $\Delta^{14}C$ (section 3.1), the adequacy of box models to analyze data from a few locations can legitimately be questioned. For instance, most of the data for the Atlantic Ocean are from the northern hemisphere (Figure 1). In this section, we consider a slightly more detailed model, where the deep Atlantic box in the original model is split into two boxes: a northern box and a southern box.

**Table 5**
*Resolvability of $\Delta^{14}C$ in the Surface Boxes for the K = 20 Solution*

| Boreal | Atlantic | Antarctic | Indian | South Pacific | North Pacific |
|---|---|---|---|---|---|
| 0.50 | 0.02 | 0.89 | 0.01 | 0.01 | 0.02 |

Volume transports in the modified model are derived from those in the original model (Figure 4). Thus, in the modified model, the northern box receives a flux of 21.5 Sv from Northern Component Water, exchanges 3.5/2 = 1.75 Sv with the Intermediate Atlantic, and loses 21.5 Sv of water to the southern box. The southern box receives a flux of 21.5 Sv from the northern box, exchanges

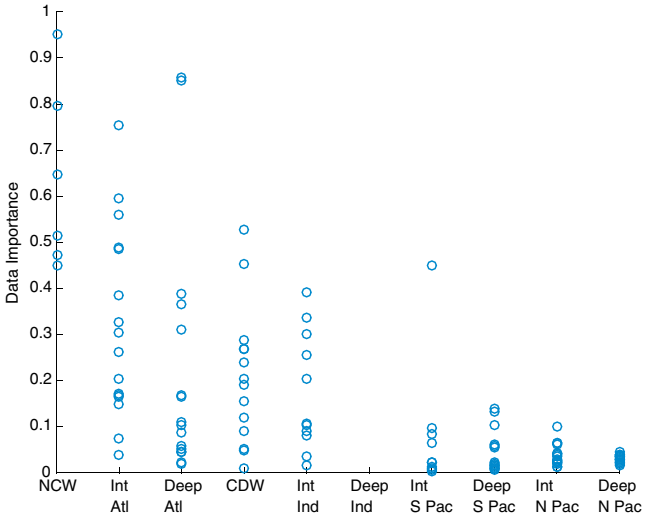


**Figure 11.** Data importance of the subsurface boxes for the case where low-$\Delta^{14}C$ records are included in the analysis. Each circle corresponds to a bin.

1.75 Sv with the Intermediate Atlantic, and loses 21.5 Sv to, and exchanges 8 Sv with, Circumpolar Deep Water. The other volume transports of the modified model are the same as in the original model. With this circulation scheme, volume is conserved in all boxes, as in the original model.

The modified model of modern ocean ventilation is fit to the deep water $\Delta^{14}C$ data using the same assumptions as for the original model (section 3.2). The fit to the deep water data is generally good (Figure S7 and Table 4), and all of the surface $\Delta^{14}C$ values are within two standard deviations of the bounds provided by the atmosphere and deep ocean data (Figure S8). Thus, the modified model displays a similar aptitude to explain the data as the original model.

### 4.4. Effect of Model Architecture: Deep and Bottom Atlantic Boxes

Recent studies have inferred the presence of $^{14}C$ age maxima at water depths of 3,500–4,500 m in the deep Atlantic during the LGM (Burke et al., 2015; Keigwin & Swift, 2017; Skinner et al., 2017). Age extrema at these depths cannot be captured by the ventilation model used in this study, as this model represents the entire Atlantic below 1,500 m with a single box. In this section, we consider another slightly more detailed model, where the Atlantic Ocean below 1,500 m is subdivided into two juxtaposed boxes: a deep box extending from 1,500 m to 3,000 m and a bottom box extending from 3,000 m to 4,000 m, the bottom depth of CYCLOPS (Figure S9).

In this modified model, the volume transports in the deep Atlantic are established as follows. The transports from NCW to the deep and bottom boxes are set to 13 Sv and 8.5 Sv, respectively, in proportion to their thicknesses. The exchange flux of 8 Sv between CDW and the bottom box represents the combined effect of (i) the northward flux of Antarctic Bottom Water (AABW) and (ii) the southward flux of the lowest components of North Atlantic Deep Water (NADW) and of entrained AABW (Lumpkin & Speer, 2007). Water flows at the rate of 8.5 Sv from the bottom box to the deep box to represent the upwelling driven by mixing below the crest of the Mid-Atlantic Ridge (Ganachaud & Wunsch, 2000; St Laurent et al., 2002; Waterhouse et al., 2014). Finally, the water flux from the deep box to CDW, set to 21.5 Sv, accounts for the main components of southward deep water export (Ganachaud & Wunsch, 2000). As for the other model versions considered in this paper, volume is conserved in all boxes.

We find that with the modified model comprising two layers in the deep Atlantic, (i) the deep water $\Delta^{14}C$ values produced from the fit still explain most of the deep water data (Figures S10 and S11 and Table 4) and (ii) the inferred surface $\Delta^{14}C$ values are all within the bounds provided by deep water and atmospheric $\Delta^{14}C$ (Figure S12). Although this model appears to overestimate some of the deep water data in the bottom Atlantic, a closer inspection of the results shows that only 1 of the 10 fitted values differ from the bin values by more than two standard deviations (Figure S10).

## 5. Paleoceanographic Implications

Radiocarbon measurements on fossil samples recovered from the seafloor have been used over the past two decades to draw inferences about changes in deep ocean ventilation during the last deglaciation. The study of ocean paleoventilation is a particularly active field of research, often motivated by its postulated effect on atmospheric $CO_2$ concentration and climate. However, interpretations of deep-sea $^{14}C$ records remain challenging, given in particular the multiple sources of error that can affect these records and the paucity of the current database (by modern standards).

In this study, we present a compilation of 1,361 deep water $\Delta^{14}C$ data originating from different oceanic basins and spanning the past 40 kyr. Notable in the compilation is the observation of a decline in deep water $\Delta^{14}C$ over the past 25 kyr in different basins, particularly if deep water $\Delta^{14}C$ records previously interpreted as reflecting seafloor processes are discarded. The deep water $\Delta^{14}C$ decline is similar to that observed in the atmospheric $\Delta^{14}C$ reconstruction over the same time interval and appears significant (Table 2).

Motivated by this result, we explore the extent to which the deep water $\Delta^{14}C$ records jointly require changes in basin-scale ventilation rates from 20 to 10 kyr B.P., a time interval characterized by a relative abundance of data. A quantitative model of modern ocean ventilation is fit to deglacial data, and the results of the fit are analyzed. These results are the fitted values of deep water $\Delta^{14}C$ and the implied values of surface water $\Delta^{14}C$. We find that most of the fit residuals (87%) are consistent with the estimated data uncertainties and that the implied values of surface water $\Delta^{14}C$ are reasonable given the bounds provided by contemporaneous values of atmospheric $\Delta^{14}C$ and deep water $\Delta^{14}C$. None of our sensitivity tests, bearing on bin width (section 4.1), consideration of low-$\Delta^{14}C$ records (section 4.2), and model architecture (sections 4.3 and 4.4), provide strong evidence that the deglacial data are incompatible with modern ocean ventilation as represented in the box model (Table 4).

Nonetheless, whereas most of the deep water $\Delta^{14}C$ data appear consistent with basin-scale ventilation rates in the modern ocean, these rates cannot account for all the data. Moreover, some of the surface water $\Delta^{14}C$ values implied by the deep water $\Delta^{14}C$ data under the assumption of modern ventilation significantly deviate from the values expected from variations in atmospheric $\Delta^{14}C$ and $pCO_2$. Four out of 32 of the implied values in the northern North Atlantic (boreal box) and the Southern Ocean (Antarctic box) differ from the expected values by more than two standard deviations (Figure 10). It is tempting to notice that a number of implied values that most strongly deviate from the expected values, albeit not always significantly so (at the level of two standard deviations), cluster in some intervals, most notably during the BA and HS1 both in the northern North Atlantic and in the Southern Ocean (Figure 10).

Estimates of deep ocean $^{14}C$ age have been used to infer variations in deep ocean carbon storage and atmospheric $CO_2$ level during the last (de)glacial periods (e.g., Sarnthein et al., 2013; Skinner et al., 2010). Our results, on the other hand, show that deep water $\Delta^{14}C$ records do not generally require basin-scale ventilation rates that are different from modern, provided that changes in surface reservoir ages occurred, particularly at high latitudes. Changes in sea ice cover at high latitudes could reconcile the inferences above with our results, because these changes can impact both air-sea $CO_2$ exchange (e.g., Stephens & Keeling, 2000) and surface reservoir ages (e.g., Bard, 1988). For example, during the BA (Antarctic Cold Reversal), sea ice in the Southern Ocean might have expanded (e.g., Ferry et al., 2015) and ice-free conditions might have existed in the northern North Atlantic (e.g., Müller et al., 2009), which could have influenced the surface $^{14}C$ disequilibria with the atmosphere (Figure 10). Whether these changes could operate without a commensurate change in basin-scale ventilation, detectable from $^{14}C$ measurements on fossil carbonates, remains to be investigated. The possibility that deep water $\Delta^{14}C$ records reflect some combination of changes in deep circulation and surface water reservoir ages cannot be ruled out based on the kinematical model used in this study.

Many studies using different proxies have concluded for deglacial changes in ocean circulation (e.g., Bryan et al., 2010; McManus et al., 2004; Rae et al., 2014; Siani et al., 2013; Skinner et al., 2014). While such conclusions are clearly plausible, it should also be stressed that quantitative estimates of the inferred circulation changes and of their uncertainties are typically not reported. Absent such estimates, the degree of (in)consistency of inferences between different studies, and between prior studies and the present study, is difficult to assess.

Importantly, our results do not imply that changes in basin-scale ocean ventilation did not take place during the deglaciation. Our approach may not have the skill to differentiate modest changes in basin-scale ventilation rates, although it should be adequate to test large changes in radiocarbon inventory (Hain et al., 2014b) and ocean circulation (e.g., Broecker & Barker, 2007; McManus et al., 2004). Furthermore, whether our results will still hold as additional deep water $\Delta^{14}C$ data become available remains to be seen. Additional data would be helpful, not only for better constraining basin-scale ventilation changes (if any) but also for identifying changes on time scales shorter than those considered in this analysis. Finally, our results do not rule out the possibility of deglacial changes in ventilation at horizontal scales smaller than O(1,000 km) and vertical scales smaller than O(1,000 m), as these scales are not resolved by the ocean model used in this study.

## 6. Perspectives

Besides the need for more data, especially in regions with currently poor spatial and (or) temporal coverage, we feel that other lines of research should be pursued in order to enhance the value of deep water radiocarbon records in the study of paleocirculations. First and foremost, accurate estimates of core and coral

chronologies are critical for the reconstruction of deep water $\Delta^{14}C$, since $\Delta^{14}C$ depends sensitively on calendar age (e.g., Davies-Walczak et al., 2014). The chronological errors arising from varying sedimentation rate and reservoir age are poorly understood and generally not reported in the publications. Second, a common procedure to obtain $\Delta^{14}C$ measurements on fossil samples appears highly desirable for the construction of an internally consistent data set. For example, $^{14}C$ measurements on benthic shells could be restricted to samples originating from peaks in benthic shell abundance (e.g., Keigwin & Schlegel, 2002) and (or) to cores with high sedimentation rates, so as to minimize bioturbation effects. Finally, studies are needed to establish the relationship between $\Delta^{14}C$ of benthic foraminifera or deep-sea corals sampled from the seafloor and the $\Delta^{14}C$ of ambient bottom water (e.g., Figure 6). In particular, more research should be done on the potential of seafloor processes, such as hydrothermal activities and methane seeps, to affect the $^{14}C/^{12}C$ ratios of fossil biogenic carbonates (e.g., Ronge et al., 2016; Stott & Timmermann, 2011).

On the other hand, it is clear that progress in the use of radiocarbon data to extract information about paleoventilation should not come exclusively from the data. Use of more complete models than the one considered here is clearly desirable. In particular, models that have sufficient spatial resolution to properly represent ocean ventilation in marginal regions where most of the paleodata lie would alleviate the need for estimating large-scale averages and increase the power of these data to constrain past ocean conditions. Use of an ocean circulation model—with an explicit representation of the equations of motion—would allow inferences to be made that are both dynamically and observationally consistent (e.g., Burke et al., 2011; Gebbie & Huybers, 2006; LeGrand & Wunsch, 1995; Marchal & Curry, 2008). Consideration of sea ice dynamics and C cycle processes, particularly at the seafloor, might also be needed for interpreting at least some of the deep water $^{14}C$ records.

Besides, other approaches of data analysis can offer complementary insights. The approach adopted in this paper does not lead to quantitative inferences about past ventilation rates but to an assessment of the changes in surface water $\Delta^{14}C$ that the deep water $\Delta^{14}C$ data imply under the assumption of modern ventilation. Alternative approaches, such as based on Lagrange multipliers (adjoint methods) and sequential methods of optimal estimation theory (Kalman filters and related smoothers), could be used to make such inferences from the quantitative combination of a model with the data (e.g., Wunsch, 2006). Each of these approaches has strengths and weaknesses. Whereas adjoint methods can be used to fit an ocean general circulation model to ocean data, they do not generally produce error estimates (e.g., Dail & Wunsch, 2014). Sequential methods do lead to the production of error estimates but are more difficult to apply given their high computational cost. As a result, sequential methods have generally been used to combine ocean data with simplified models (e.g., Marchal et al., 2016).

**Acknowledgments**

O. M. thanks Edouard Bard for sharing preindustrial estimates of radiocarbon reservoir ages. Discussions with Dave Lund and Laura Robinson helped the authors to stay updated with the paleo-$\Delta^{14}C$ database and with potential issues in some $\Delta^{14}C$ records. Carl Wunsch and two referees provided useful comments on an early version of the manuscript. The authors are grateful to Mathis Hain and an anonymous reviewer for their thoughtful and constructive comments on the present manuscript. This research was supported by a grant from the U.S. National Science Foundation (OCE-1301907). Data used in this study are archived at the NOAA National Climatic Data Center (https://www.ncdc.noaa.gov/paleo/study/21390).

## References

Adkins, J. F., Cheng, H., Boyle, E. A., Druffel, E. R., & Edwards, R. L. (1998). Deep-sea coral evidence for rapid change in ventilation of the deep North Atlantic 15,400 years ago. *Science*, *280*(5364), 725–728. https://doi.org/10.1126/science.280.5364.725

Ahagon, N., Ohkushi, K. I., Uchida, M., & Mishima, T. (2003). Mid-depth circulation in the northwest Pacific during the last deglaciation: Evidence from foraminiferal radiocarbon ages. *Geophysical Research Letters*, *30*(21), 2097. https://doi.org/10.1029/2003GL018287

Amrhein, D. E., Gebbie, G., Marchal, O., & Wunsch, C. (2015). Inferring surface water equilibrium calcite $\delta^{18}O$ during the last deglacial period from benthic foraminiferal records: Implications for ocean circulation. *Paleoceanography*, *30*, 1470–1489. https://doi.org/10.1002/2014PA002743

Anderson, R. F., Ali, S., Bradtmiller, L. I., Nielsen, S. H. H., Fleisher, M. Q., Anderson, B. E., & Burckle, L. H. (2009). Wind-driven upwelling in the Southern Ocean and the deglacial rise in atmospheric $CO_2$. *Science*, *323*, 1443–1448. https://doi.org/10.1126/science.1167441

Andree, M., Oeschger, H., Broecker, W., Beavan, N., Klas, M., Mix, A., … Peng, T.-H. (1986). Limits on the ventilation rate for the deep ocean over the last 12,000 years. *Climate Dynamics*, *1*(1), 53–62. https://doi.org/10.1007/BF01277046

Audi, G., Bersillon, O., Blachot, J., & Wapstra, A. H. (2003). The NUBASE evaluation of nuclear and decay properties. *Nuclear Physics A*, *729*(1), 3–128. https://doi.org/10.1016/j.nuclphysa.2003.11.001

Bard, E. (1988). Correction of accelerator mass spectrometry $^{14}C$ ages measured in planktonic foraminifera: Paleoceanographic implications. *Paleoceanography*, *3*(6), 635–645. https://doi.org/10.1029/PA003i006p00635

Barker, S., Knorr, G., Vautravers, M. J., Diz, P., & Skinner, L. C. (2010). Extreme deepening of the Atlantic overturning circulation during deglaciation. *Nature Geoscience*, *3*, 567–571. https://doi.org/10.1038/ngeo921

Broecker, W., & Barker, S. (2007). A 190‰ drop in atmosphere's $\Delta^{14}C$ during the "Mystery Interval" (17.5 to 14.5 kyr). *Earth and Planetary Science Letters*, *256*, 90–99. https://doi.org/10.1016/j.epsl.2007.01.015

Broecker, W., & Clark, E. (2010). Search for a glacial-age $^{14}C$-depleted ocean reservoir. *Geophysical Research Letters*, *37*, L13606. https://doi.org/10.1029/2010GL043969

Broecker, W. S., & Peng, T.-H. (1982). *Tracers in the Sea* (690 pp.). Palisades, New York: Lamont-Doherty Geological Observatory.

Broecker, W., Andree, M., Bonani, G., Wolfli, W., Oeschger, H., Klas, M., … Curry, W. (1988). Preliminary estimates for the radiocarbon age of deep water in the glacial ocean. *Paleoceanography*, *3*(6), 659–669. https://doi.org/10.1029/PA003i006p00659

Broecker, W., Klas, M., Ragano-Beavan, N., Mathieu, G., Mix, A., Andree, M., … Morenzoni, E. (1988). Accelerator mass spectrometry radiocarbon measurements on marine carbonate samples. *Radiocarbon*, *30*(03), 261–263. https://doi.org/10.1017/S0033822200044234

Broecker, W. S., Klas, M., Clark, E., Trumbore, S. E., Bonani, G., Wölfli, W., & Ivy, S. (1990). AMS radiocarbon measurements on foraminifera shells from deep-sea cores. *Radiocarbon*, *32*(02), 119–133. https://doi.org/10.1017/S003382220004011X

Broecker, W. S., Peng, T.-H., Trumbore, S., Bonani, G., & Wolfli, W. (1990). The distribution of radiocarbon in the glacial ocean. *Global Biogeochemical Cycles*, *4*(1), 103–117. https://doi.org/10.1029/GB004i001p00103

Broecker, W., Barker, S., Clark, E., Hajdas, I., Bonani, G., & Stott, L. (2004). Ventilation of the glacial deep Pacific Ocean. *Science*, *306*, 1169–1172. https://doi.org/10.1126/science.1102293

Broecker, W., Clark, E., & Barker, S. (2008). Near constancy of the Pacific Ocean surface to mid-depth radiocarbon-age difference over the last 20 kyr. *Earth and Planetary Science Letters*, *274*, 322–326. https://doi.org/10.1016/j.epsl.2008.07.035

Bryan, S. P., Marchitto, T. M., & Lehman, S. J. (2010). The release of $^{14}$C-depleted carbon from the deep ocean during the last deglaciation: Evidence from the Arabian Sea. *Earth and Planetary Science Letters*, *298*, 244–254. https://doi.org/10.1016/j.epsl.2010.08.025

Burke, A., & Robinson, L. F. (2012). The Southern Ocean's role in carbon exchange during the last deglaciation. *Science*, *335*(6068), 557–561. https://doi.org/10.1126/science.1208163

Burke, A., Marchal, O., Bradtmiller, L. I., McManus, J. F., & François, R. (2011). Application of an inverse method to interpret $^{231}$Pa/$^{230}$Th observations from marine sediments. *Paleoceanography*, *26*, PA1212. https://doi.org/10.1029/2010PA002022

Burke, A., Stewart, A. L., Adkins, J. F., Ferrari, R., Jansen, M. F., & Thompson, A. F. (2015). The glacial mid-depth radiocarbon bulge and its implications for the overturning circulation. *Paleoceanography*, *30*, 1021–1039. https://doi.org/10.1002/2015PA002778

Cao, L., Fairbanks, R. G., Mortlock, R. A., & Risk, M. J. (2007). Radiocarbon reservoir age of high latitude North Atlantic surface water during the last deglacial. *Quaternary Science Reviews*, *26*, 732–742. https://doi.org/10.1016/j.quascirev.2006.10.001

Chen, T., Robinson, L. F., Burke, A., Southon, J., Spooner, P., Morris, P. J., & Ng, H. C. (2015). Synchronous centennial abrupt events in the ocean and atmosphere during the last deglaciation. *Science*, *349*(6255), 1537–1541. https://doi.org/10.1126/science.aac6159

Clark, P. U., Dyke, A. S., Shakun, J. D., Carlson, A. E., Clark, J., Wohlfarth, B., … McCabe, A. M. (2009). The Last Glacial Maximum. *Science*, *325*, 710–714. https://doi.org/10.1126/science.1172873

Cléroux, C., deMenocal, P., & Guilderson, T. (2011). Deglacial radiocarbon history of tropical Atlantic thermocline waters: Absence of $CO_2$ reservoir purging signal. *Quaternary Science Reviews*, *30*, 1875–1882. https://doi.org/10.1016/j.quascirev.2011.04.015

Cook, M. S., & Keigwin, L. D. (2015). Radiocarbon profiles of the NW Pacific from the LGM and deglaciation: Evaluating ventilation metrics and the effect of uncertain surface reservoir ages. *Paleoceanography*, *30*, 174–195. https://doi.org/10.1002/2014PA002649

Dail, H., & Wunsch, C. (2014). Dynamical reconstruction of upper-ocean conditions in the Last Glacial Maximum Atlantic. *Journal of Climate*, *27*(2), 807–823. https://doi.org/10.1175/JCLI-D-13-00211.1

Davies-Walczak, M., Mix, A. C., Stoner, J. S., Southon, J. R., Cheseby, M., & Xuan, C. (2014). Late Glacial to Holocene radiocarbon constraints on North Pacific Intermediate Water ventilation and deglacial atmospheric $CO_2$ sources. *Earth and Planetary Science Letters*, *397*, 57–66. https://doi.org/10.1016/j.epsl.2014.04.004

de la Fuente, M., Skinner, L., Calvo, E., Pelejero, C., & Cacho, I. (2015). Increased reservoir ages and poorly ventilated deep waters inferred in the glacial Eastern Equatorial Pacific. *Nature Communications*, *6*, 7420. https://doi.org/10.1038/ncomms8420

De Pol-Holz, R., Keigwin, L., Southon, J., Hebbeln, D., & Mohtadi, M. (2010). No signature of abyssal carbon in intermediate waters off Chile during deglaciation. *Nature Geoscience*, *3*, 192–195. https://doi.org/10.1038/ngeo745

Duplessy, J.-C., Arnold, M., Bard, E., Juillet-Leclerc, A., Kallel, N., & Labeyrie, L. (1989). AMS $^{14}$C study of transient events and of the ventilation rate of the Pacific intermediate water during the last deglaciation. *Radiocarbon*, *31*(03), 493–502. https://doi.org/10.1017/S003382220001208X

Eltgroth, S. F., Adkins, J. F., Robinson, L. F., Southon, J., & Kashgarian, M. (2006). A deep-sea coral record of North Atlantic radiocarbon through the Younger Dryas: Evidence for intermediate water/deepwater reorganization. *Paleoceanography*, *21*, PA4207. https://doi.org/10.1029/2005PA001192

Ferry, A. J., Crosta, X., Quilty, P. G., Fink, D., Howard, W., & Armand, L. K. (2015). First records of winter sea ice concentration in the southwest Pacific sector of the Southern Ocean. *Paleoceanography*, *30*, 1525–1539. https://doi.org/10.1002/2014PA002764

Fiadeiro, M. E. (1982). Three-dimensional modeling of tracers in the deep Pacific Ocean II. Radiocarbon and the circulation. *Journal of Marine Research*, *40*, 537–550.

Fischer, H., Schmitt, J., Lüthi, D., Stocker, T. F., Tschumi, T., Parekh, P., … Wolff, E. (2010). The role of Southern Ocean processes in orbital and millennial $CO_2$ variations—A synthesis. *Quaternary Science Reviews*, *29*, 193–205. https://doi.org/10.1016/j.quascirev.2009.06.007

Freeman, E., Skinner, L. C., Tisserand, A., Dokken, T., Timmermann, A., Menviel, L., & Friedrich, T. (2015). An Atlantic–Pacific ventilation seesaw across the last deglaciation. *Earth and Planetary Science Letters*, *424*, 237–244. https://doi.org/10.1016/j.epsl.2015.05.032

Freeman, E., Skinner, L. C., Waelbroeck, C., & Hodell, D. (2016). Radiocarbon evidence for enhanced respired carbon storage in the Atlantic at the Last Glacial aximum. *Nature Communications*, *7*, 11998. https://doi.org/10.1038/ncomms11998

Galbraith, E. D., Jaccard, S. L., Pedersen, T. F., Sigman, D. M., Haug, G. H., Cook, M., … François, R. (2007). Carbon dioxide release from the North Pacific abyss during the last deglaciation. *Nature*, *449*, 890–893. https://doi.org/10.1038/nature06227

Galbraith, E. D., Kwon, E. Y., Bianchi, D., Hain, M. P., & Sarmiento, J. L. (2015). The impact of atmospheric $pCO_2$ on carbon isotope ratios of the atmosphere and ocean. *Global Biogeochemical Cycles*, *29*, 307–324. https://doi.org/10.1002/2014GB004929

Ganachaud, A., & Wunsch, C. (2000). Improved estimates of global ocean circulation, heat transport and mixing from hydrographic data. *Nature*, *408*(6811), 453–457. https://doi.org/10.1038/35044048

Gebbie, G. (2012). Tracer transport timescales and the observed Atlantic-Pacific lag in the timing of the Last Termination. *Paleoceanography*, *27*, PA3225. https://doi.org/10.1029/2011PA002273

Gebbie, G., & Huybers, P. (2006). Meridional circulation during the Last Glacial Maximum explored through a combination of South Atlantic $\delta^{18}$O observations and a geostrophic inverse model. *Geochemistry, Geophysics, Geosystems*, *7*, Q11N07. https://doi.org/10.1029/2006GC001383

Gebhardt, H., Sarnthein, M., Grootes, P. M., Kiefer, T., Kuehn, H., Schmieder, F., & Röhl, U. (2008). Paleonutrient and productivity records from the subarctic North Pacific for Pleistocene glacial terminations I to V. *Paleoceanography*, *23*, PA4212. https://doi.org/10.1029/2007PA001513

Goldstein, S. J., Lea, D. W., Chakraborty, S., Kashgarian, M., & Murrell, M. T. (2001). Uranium-series and radiocarbon geochronology of deep-sea corals: Implications for Southern Ocean ventilation rates and the oceanic carbon cycle. *Earth and Planetary Science Letters*, *193*(1-2), 167–182. https://doi.org/10.1016/S0012-821X(01)00494-0

Gorbarenko, S. A., Khusid, T. A., Basov, I. A., Oba, T., Southon, J. R., & Koizumi, I. (2002). Glacial Holocene environment of the southeastern Okhotsk Sea: Evidence from geochemical and palaeontological data. *Palaeogeography, Palaeoclimatology, Palaeoecology*, *177*(3-4), 237–263. https://doi.org/10.1016/S0031-0182(01)00335-2

Gorbarenko, S. A., Southon, J. R., Keigwin, L. D., Cherepanova, M. V., & Gvozdeva, I. G. (2004). Late Pleistocene-Holocene oceanographic variability in the Okhotsk Sea: Geochemical, lithological and paleontological evidence. *Palaeogeography, Palaeoclimatology, Palaeoecology*, *209*(1-4), 281–301. https://doi.org/10.1016/j.palaeo.2004.02.013

Gorbarenko, S. A., Psheneva, O. Y., Artemova, A. V., Tiedemann, R., & Nürnberg, D. (2010). Paleoenvironment changes in the NW Okhotsk Sea for the last 18 kyr determined with micropaleontological, geochemical, and lithological data. *Deep Sea Research Part I: Oceanographic Research Papers*, *57*, 797–811. https://doi.org/10.1016/j.dsr.2010.04.004

Gottschalk, J., Skinner, L. C., Lippold, J., Vogel, H., Frank, N., Jaccard, S. L., & Waelbroeck, C. (2016). Biological and physical controls in the Southern Ocean on past millennial-scale atmospheric $CO_2$ changes. *Nature Communications*, *7*, 11539. https://doi.org/10.1038/ncomms11539

Hain, M. P., Sigman, D. M., & Haug, G. H. (2010). Carbon dioxide effects of Antarctic stratification, North Atlantic Intermediate Water formation, and subantarctic nutrient drawdown during the last ice age: Diagnosis and synthesis in a geochemical box model. *Global Biogeochemical Cycles*, *24*, GB4023. https://doi.org/10.1029/2010GB003790

Hain, M. P., Sigman, D. M., & Haug, G. H. (2011). Shortcomings of the isolated abyssal reservoir model for deglacial radiocarbon changes in the mid-depth Indo-Pacific Ocean. *Geophysical Research Letters*, *38*, L04604. https://doi.org/10.1029/2010GL046158

Hain, M. P., Sigmal, D. M., & Haug, G. H. (2014a). The biological pump in the past. *Treatise on Geochemistry (Second Edition)*, *8*, 485–517.

Hain, M. P., Sigman, D. M., & Haug, G. H. (2014b). Distinct roles of the Southern Ocean and North Atlantic in the deglacial atmospheric radiocarbon decline. *Earth and Planetary Science Letters*, *394*, 198–208. https://doi.org/10.1016/j.epsl.2014.03.020

Hines, S. K. V., Southon, J. R., & Adkins, J. F. (2015). A high-resolution record of Southern Ocean intermediate water radiocarbon over the past 30,000 years. *Earth and Planetary Science Letters*, *432*, 46–58. https://doi.org/10.1016/j.epsl.2015.09.038

Ikehara, K., Ohkushi, K. I., Shibahara, A., & Hoshiba, M. (2006). Change of bottom water conditions at intermediate depths of the Oyashio region, NW Pacific over the past 20,000 yrs. *Global and Planetary Change*, *53*, 78–91. https://doi.org/10.1016/j.gloplacha.2006.01.011

Ikehara, K., Danhara, T., Yamashita, T., Tanahashi, M., Morita, S., & Ohkushi, K. I. (2011). Paleoceanographic control on a large marine reservoir effect offshore of Tokai, south of Japan, NW Pacific, during the last glacial maximum-deglaciation. *Quaternary International*, *246*, 213–221. https://doi.org/10.1016/j.quaint.2011.07.005

Ingram, B. I., & Kennett, J. P. (1995). Radiocarbon chronology and planktonic-benthic foraminiferal $^{14}C$ age differences in Santa Barbara Basin sediments, Hole 893A. *Proceedings of the Ocean Drilling Program, Scientific Results*, *146*(Part 2), 19–27.

Jaccard, S. L., Galbraith, E. D., Martínez-García, A., & Anderson, R. F. (2016). Covariation of deep Southern Ocean oxygenation and atmospheric $CO_2$ through the last ice age. *Nature*, *530*(7589), 207–210. https://doi.org/10.1038/nature16514

Keigwin, L. D. (2002). Late Pleistocene-Holoicene paleoceanography and ventilation of the Gulf of California. *Journal of Oceanography*, *58*(2), 421–432. https://doi.org/10.1023/A:1015830313175

Keigwin, L. D. (2004). Radiocarbon and stable isotope constraints on Last Glacial Maximum and Younger Dryas ventilation in the western North Atlantic. *Paleoceanography*, *19*, PA4012. https://doi.org/10.1029/2004PA001029

Keigwin, L. D., & Boyle, E. A. (2008). Did North Atlantic overturning halt 17,000 years ago? *Paleoceanography*, *23*, PA1101. https://doi.org/10.1029/2007PA001500

Keigwin, L. D., & Lehman, S. J. (2015). Radiocarbon evidence for a possible abyssal front near 3.1 km in the glacial equatorial Pacific Ocean. *Earth and Planetary Science Letters*, *425*, 93–104. https://doi.org/10.1016/j.epsl.2015.05.025

Keigwin, L., & Schlegel, M. (2002). Ocean ventilation and sedimentation since the glacial maximum at 3 km in the western North Atlantic. *Geochemistry, Geophysics, Geosystems*, *3*(6), 1034. https://doi.org/10.1029/2001GC000283

Keigwin, L. D., & Swift, S. A. (2017). Carbon isotope evidence for a northern source of deep water in the glacial western North Atlantic. *Proceedings of the National Academy of Sciences*, *114*(11), 2831–2835. https://doi.org/10.1073/pnas.1614693114

Keir, R. S. (1988). On the Late Pleistocene Ocean geochemistry and circulation. *Paleoceanography*, *3*, 413–445.

Kendall, M., & Gibbons, J. D. R. (1990). *Rank Correlation Methods*. Oxford: Oxford University Press.

Key, R. M., Kozyr, A., Sabine, C. L., Lee, K., Wanninkhof, R., Bullister, J. L., … Peng, T.-H. (2004). A global ocean carbon climatology: Results from Global Data Analysis Project (GLODAP). *Global Biogeochemical Cycles*, *18*, GB4031. https://doi.org/10.1029/2004GB002247

Knox, F., & McElroy, M. B. (1984). Changes in atmospheric $CO_2$: Influence of the marine biota at high latitude. *Journal of Geophysical Research*, *89*(D3), 4629–4637. https://doi.org/10.1029/JD089iD03p04629

Lambeck, K., Rouby, H., Purcell, A., Sun, Y., & Sambridge, M. (2014). Sea level and global ice volumes from the Last Glacial Maximum to the Holocene. *Proceedings of the National Academy of Sciences*, *111*(43), 15,296–15,303. https://doi.org/10.1073/pnas.1411762111

LeGrand, P., & Wunsch, C. (1995). Constraints from paleotracer data on the North Atlantic circulation during the Last Glacial Maximum. *Paleoceanography*, *10*(6), 1011–1045. https://doi.org/10.1029/95PA01455

Lindsay, C. M., Lehman, S. J., Marchitto, T. M., Carriquiry, J. D., & Ortiz, J. D. (2016). New constraints on deglacial marine radiocarbon anomalies from a depth transect near Baja California. *Paleoceanography*, *31*, 1103–1116. https://doi.org/10.1002/2015PA002878

Lumpkin, R., & Speer, K. (2003). Large-scale vertical and horizontal circulation in the North Atlantic Ocean. *Journal of Physical Oceanography*, *33*(9), 1902–1920. https://doi.org/10.1175/1520-0485(2003)033%3C1902:LVAHCI%3E2.0.CO;2

Lumpkin, R., & Speer, K. (2007). Global ocean meridional overturning. *Journal of Physical Oceanography*, *37*, 2550–2562. https://doi.org/10.1175/JPO3130.1

Lumpkin, R., Speer, K. G., & Koltermann, K. P. (2008). Transport across 48°N in the Atlantic Ocean. *Journal of Physical Oceanography*, *38*, 733–752. https://doi.org/10.1175/2007JPO3636.1

Lund, D. C., & Asimow, P. D. (2011). Does sea level influence mid-ocean ridge magmatism on Milankovitch timescales? *Geochemistry, Geophysics, Geosystems*, *12*, Q12009. https://doi.org/10.1029/2011GC003693

Lund, D. C., Mix, A. C., & Southon, J. (2011). Increased ventilation age of the deep northeast Pacific Ocean during the last deglaciation. *Nature Geoscience*, *4*, 771–774. https://doi.org/10.1038/ngeo1272

Lund, D. C., Tessin, A. C., Hoffman, J. L., & Schmittner, A. (2015). Southwest Atlantic water mass evolution during the last deglaciation. *Paleoceanography*, *30*, 477–494. https://doi.org/10.1002/2014PA002657

Magana, A. L., Southon, J. R., Kennett, J. P., Roark, E. B., Sarnthein, M., & Stott, L. D. (2010). Resolving the cause of large differences between deglacial benthic foraminifera radiocarbon measurements in Santa Barbara Basin. *Paleoceanography*, *25*, PA4102. https://doi.org/10.1029/2010PA002011

Mangini, A., Lomitschka, M., Eichstädter, R., Frank, N., Vogler, S., Bonani, G., … Patzold, J. (1998). Coral provides way to age deep water. *Nature*, *392*(6674), 347–348. https://doi.org/10.1038/32804

Mangini, A., Godoy, J. M., Godoy, M. L., Kowsmann, R., Santos, G. M., Ruckelshausen, M., … Wacker, L. (2010). Deep sea corals off Brazil verify a poorly ventilated Southern Pacific Ocean during H2, H1 and the Younger Dryas. *Earth and Planetary Science Letters*, *293*, 269–276. https://doi.org/10.1016/j.epsl.2010.02.041

Marchal, O., & Curry, W. B. (2008). On the abyssal circulation in the glacial Atlantic. *Journal of Physical Oceanography*, *38*, 2014–2037. https://doi.org/10.1175/2008JPO3895.1

Marchal, O., Stocker, T. F., & Joos, F. (1999). Physical and biogeochemical responses to freshwater-induced thermohaline variability in a zonally averaged ocean model. In P. U. Clark, R. S. Webb, & L. D. Keigwin (Eds.), *Mechanisms of Global Climate Change at Millennial Time Scales* (pp. 263–284). Washington, DC: American Geophysical Union. https://doi.org/10.1029/GM112p0263

Marchal, O., Waelbroeck, C., & Colin de Verdière, A. (2016). On the movements of the North Atlantic subpolar front in the preinstrumental past. *Journal of Climate*, *29*(4), 1545–1571. https://doi.org/10.1175/JCLI-D-15-0509.1

Marchitto, T. M., Lehman, S. J., Ortiz, J. D., Fluckiger, J., & van Geen, A. (2007). Marine radiocarbon evidence for the mechanism of deglacial atmospheric $CO_2$ rise. *Science*, *316*, 1456–1459. https://doi.org/10.1126/science.1138679

Marshall, J., & Speer, K. (2012). Closure of the meridional overturning circulation through Southern Ocean upwelling. *Nature Geoscience*, *5*(3), 171–180. https://doi.org/10.1038/ngeo1391

Max, L., Lembke-Jene, L., Riethdorf, J.-R., Tiedemann, R., Nürnberg, D., Kühn, H., & Mackensen, A. (2014). Pulses of enhanced North Pacific Intermediate Water ventilation from the Okhotsk Sea and Bering Sea during the last deglaciation. *Climate of the Past*, *10*(2), 591–605. https://doi.org/10.5194/cp-10-591-2014

McKay, J. L., Pedersen, T. F., & Southon, J. (2005). Intensification of the oxygen minimum zone in the northeast Pacific off Vancouver Island during the last deglaciation: Ventilation and/or export production? *Paleoceanography*, *20*, PA4002. https://doi.org/10.1029/2003PA000979

McManus, J. F., François, R., Gherardi, J.-M., Keigwin, L. D., & Brown-Leger, S. (2004). Collapse and rapid resumption of Atlantic meridional circulation linked to deglacial climate changes. *Nature*, *428*, 834–837. https://doi.org/10.1038/nature02494

McNichol, A. P., Jull, A. J. T., & Burr, G. S. (2001). Converting AMS data to radiocarbon values: Considerations and conventions. *Radiocarbon*, *43*(2A), 313–320. https://doi.org/10.1017/S0033822200038169

Minoshima, K., Kawahata, H., Irino, T., Ikehara, K., Aoki, K., Uchida, M., … Shibata, Y. (2007). Deep water ventilation in the northwestern North Pacific during the last deglaciation and the early Holocene (15–5 cal. kyr B. P.) based on AMS $^{14}C$ dating. *Nuclear Instruments and Methods in Physics Research Section B: Beam Interactions with Materials and Atoms*, *259*(1), 448–452. https://doi.org/10.1016/j.nimb.2007.01.225

Mix, A. C., Lund, D. C., Pisias, N. G., Boden, P., Bornmalm, L., Lyle, M., & Pike, J. (1999). Rapid climate oscillations in the northeast Pacific during the last deglaciation reflect northern and southern hemisphere sources. In P. U. Clark, R. S. Webb, & L. D. Keigwin (Eds.), *Mechanisms of Global Climate Change at Millennial Time Scales* (pp. 127–148). Washington, DC: American Geophysical Union. https://doi.org/10.1029/GM112p0127

Monnin, E., Indermühle, A., Dällenbach, A., Flückiger, J., Stauffer, B., Stocker, T. F., … Barnola, J.-M. (2001). Atmospheric $CO_2$ concentrations over the last glacial termination. *Science*, *291*(5501), 112–114. https://doi.org/10.1126/science.291.5501.112

Müller, J., Massé, G., Stein, R., & Belt, S. T. (2009). Variability of sea-ice conditions in the Fram Strait over the past 30,000 years. *Nature Geoscience*, *2*, 772–776. https://doi.org/10.1038/ngeo665

Okazaki, Y., Timmermann, A., Menviel, L., Harada, N., Abe-Ouchi, A., Chikamoto, M. O., … Asahi, H. (2010). Deepwater formation in the North Pacific during the last glacial termination. *Science*, *329*, 200–204. https://doi.org/10.1126/science.1190612

Okazaki, Y., Sagawa, T., Asahi, H., Horikawa, K., & Onodera, J. (2012). Ventilation changes in the western North Pacific since the last glacial period. *Climate of the Past*, *8*, 17–24. https://doi.org/10.5194/cp-8-17-2012

Okazaki, Y., Kimoto, K., Asahi, H., Sato, M., Nakamura, Y., & Harada, N. (2014). Glacial to deglacial ventilation and productivity changes in the southern Okhotsk Sea. *Palaeogeography, Palaeoclimatology, Palaeoecology*, *395*, 53–66. https://doi.org/10.1016/j.palaeo.2013.12.013

Rae, J. W. B., Sarnthein, M., Foster, G. L., Ridgwell, A., Grootes, P. M., & Elliott, T. (2014). Deep water formation in the North Pacific and deglacial $CO_2$ rise. *Paleoceanography*, *29*, 645–667. https://doi.org/10.1002/2013PA002570

Rasmussen, S. O., Andersen, K. K., Svensson, A. M., Steffensen, J. P., Vinther, B. M., Clausen, H. B., … Ruth, U. (2006). A new Greenland ice core chronology for the last glacial termination. *Journal of Geophysical Research*, *111*, D06102. https://doi.org/10.1029/2005JD006079

Rasmussen, S. O., Seierstad, I. K., Andersen, K. K., Bigler, M., Dahl-Jensen, D., & Johnsen, S. J. (2008). Synchronization of the NGRIP, GRIP, and GISP2 ice cores across MIS 2 and palaeoclimatic implications. *Quaternary Science Reviews*, *27*, 18–28. https://doi.org/10.1016/j.quascirev.2007.01.016

Rayner, D., Hirschi, J. J. M., Kanzow, T., Johns, W. E., Wright, P. G., Frajka-Williams, E., … Cunningham, S. A. (2011). Monitoring the Atlantic meridional overturning circulation. *Deep Sea Research Part II: Topical Studies in Oceanography*, *58*, 1744–1753. https://doi.org/10.1016/j.dsr2.2010.10.056

Reimer, P. J., Bard, E., Bayliss, A., Beck, J. W., Blackwell, P. G., Ramsey, C. B., … van der Plicht, J. (2013). IntCal13 and Marine13 radiocarbon age calibration curves 0–50,000 years cal BP. *Radiocarbon*, *55*(04), 1869–1887. https://doi.org/10.2458/azu_js_rc.55.16947

Robinson, L. F., & van de Flierdt, T. (2009). Southern Ocean evidence for reduced export of North Atlantic Deep Water during Heinrich event 1. *Geology*, *37*, 195–198. https://doi.org/10.1130/G25363A.1

Robinson, L. F., Adkins, J. F., Keigwin, L. D., Southon, J., Fernandez, D. P., Wang, S., & Scheirer, D. S. (2005). Radiocarbon variability in the western North Atlantic during the last deglaciation. *Science*, *310*, 1469–1473. https://doi.org/10.1126/science.1114832

Robinson, L. F., Adkins, J. F., Fernandez, D. P., Burnett, D. S., Wang, S. L., Gagnon, A. C., & Krakauer, N. (2006). Primary U distribution in scleractinian corals and its implications for U series dating. *Geochemistry, Geophysics, Geosystems*, *7*, Q05022. https://doi.org/10.1029/2005GC001138

Ronge, T. A., Tiedemann, R., Lamy, F., Köhler, P., Alloway, B. V., De Pol-Holz, R., … Wacker, L. (2016). Radiocarbon constraints on the extent and evolution of the South Pacific glacial carbon pool. *Nature Communications*, *7*, 11487. https://doi.org/10.1038/ncomms11487

Rose, K. A., Sikes, E. L., Guilderson, T. P., Shane, P., Hill, T. M., Zahn, R., & Spero, H. J. (2010). Upper-ocean-to-atmosphere radiocarbon offsets imply fast deglacial carbon dioxide release. *Nature*, *466*, 1093–1097. https://doi.org/10.1038/nature09288

Sarmiento, J. L., & Gruber, N. (2006). *Ocean biogeochemical dynamics*. Princeton, NJ: Princeton University Press.

Sarmiento, J. L., & Toggweiler, J. R. (1984). A new model for the role of the oceans in determining atmospheric $pCO_2$. *Nature*, *308*(5960), 621–624. https://doi.org/10.1038/308621a0

Sarnthein, M., Kiefer, T., Grootes, P. M., Elderfield, H., & Erlenkeuser, H. (2006). Warmings in the far northwestern Pacific promoted pre-Clovis immigration to America during Heinrich event 1. *Geology*, *34*, 141–144. https://doi.org/10.1130/G22200.1

Sarnthein, M., Grootes, P. M., Kennett, J. P., & Nadeau, M. J. (2007). $^{14}C$ reservoir ages show deglacial changes in ocean currents and carbon cycle. In A. Schmittner, J. C. H. Chiang, & S. R. Hemming (Eds.), *Ocean circulation: Mechanisms and impacts—Past and future changes of*

*meridional overturning*, *Geophysical Monograph Series* (Vol. 173, pp. 175–196). Washington, DC: American Geophysical Union. https://doi.org/10.1029/173GM13

Sarnthein, M., Grootes, P. M., Holbourn, A., Kuhnt, W., & Kühn, H. (2011). Tropical warming in the Timor Sea led deglacial Antarctic warming and atmospheric $CO_2$ rise by more than 500 yr. *Earth and Planetary Science Letters*, *302*, 337–348. https://doi.org/10.1016/j.epsl.2010.12.021

Sarnthein, M., Schneider, B., & Grootes, P. M. (2013). Peak glacial $^{14}C$ ventilation ages suggest major draw-down of carbon into the abyssal ocean. *Climate of the Past*, *9*, 2595–2614. https://doi.org/10.5194/cp-9-2595-2013

Sarnthein, M., Balmer, S., Grootes, P., & Mudelsee, M. (2015). Planktic and benthic $^{14}C$ reservoir ages for three ocean basins, calibrated by a suite of $^{14}C$ plateaus in the glacial-to-deglacial Suigetsu atmospheric $^{14}C$ record. *Radiocarbon*, *57*(01), 129–151. https://doi.org/10.2458/azu_rc.57.17916

Schmitt, J., Schneider, R., Elsig, J., Leuenberger, D., Lourantou, A., Chappellaz, J., … Fischer, H. (2012). Carbon isotope constraints on the deglacial $CO_2$ rise from ice cores. *Science*, *336*, 711–714. https://doi.org/10.1126/science.1217161

Schroder-Ritzrau, A., Mangini, A., & Lomitschka, M. (2003). Deep-sea corals evidence periodic reduced ventilation in the North Atlantic during the LGM/Holocene transition. *Earth and Planetary Science Letters*, *216*(3), 399–410. https://doi.org/10.1016/S0012-821X(03)00511-9

Shackleton, N. J., Duplessy, J. C., Arnold, M., Maurice, P., Hall, M. A., & Cartlidge, J. (1988). Radiocarbon age of last glacial Pacific deep water. *Nature*, *335*(6192), 708–711. https://doi.org/10.1038/335708a0

Siani, G., Michel, E., De Pol-Holz, R., DeVries, T., Lamy, F., Carel, M., … Lourantou, A. (2013). Carbon isotope records reveal precise timing of enhanced Southern Ocean upwelling during the last deglaciation. *Nature Communications*, *4*, 2758. https://doi.org/10.1038/ncomms3758

Siegenthaler, U., & Wenk, T. (1984). Rapid atmospheric $CO_2$ variations and ocean circulation. *Nature*, *308*(5960), 624–626. https://doi.org/10.1038/308624a0

Sigman, D. M., McCorkle, D. C., & Martin, W. R. (1998). The calcite lysocline as a constraint on glacial/interglacial low-latitude production changes. *Global Biogeochemical Cycles*, *12*(3), 409–427. https://doi.org/10.1029/98GB01184

Sigman, D. M., Hain, M. P., & Haug, G. H. (2010). The polar ocean and glacial cycles in atmospheric $CO_2$ concentration. *Nature*, *466*, 47–55. https://doi.org/10.1038/nature09149

Sikes, E. L., Samson, C. R., Guilderson, T. P., & Howard, W. R. (2000). Old radiocarbon ages in the southwest Pacific Ocean during last glacial period and deglaciation. *Nature*, *405*(6786), 555–559. https://doi.org/10.1038/35014581

Sikes, E. L., Cook, M. S., & Guilderson, T. P. (2016). Reduced deep ocean ventilation in the Southern Pacific Ocean during the last glaciation persisted into the deglaciation. *Earth and Planetary Science Letters*, *438*, 130–138. https://doi.org/10.1016/j.epsl.2015.12.039

Skinner, L. C., & Shackleton, N. J. (2004). Rapid transient changes in northeast Atlantic deep water ventilation age across Termination I. *Paleoceanography*, *19*, PA2005. https://doi.org/10.1029/2003PA000983

Skinner, L. C., Fallon, S., Waelbroeck, C., Michel, E., & Barker, S. (2010). Ventilation of the deep Southern Ocean and deglacial $CO_2$ rise. *Science*, *328*, 1147–1151. https://doi.org/10.1126/science.1183627

Skinner, L. C., Waelbroeck, C., Scrivner, A. E., & Fallon, S. J. (2014). Radiocarbon evidence for alternating northern and southern sources of ventilation of the deep Atlantic carbon pool during the last deglaciation. *Proceedings of the National Academy of Sciences*, *111*(15), 5480–5484. https://doi.org/10.1073/pnas.1400668111

Skinner, L., McCave, I. N., Carter, L., Fallon, S., Scrivner, A. E., & Primeau, F. (2015). Reduced ventilation and enhanced magnitude of the deep Pacific carbon pool during the last glacial period. *Earth and Planetary Science Letters*, *411*, 45–52. https://doi.org/10.1016/j.epsl.2014.11.024

Skinner, L. C., Primeau, F., Freeman, E., de la Fuente, M., Goodwin, P. A., Gottschalk, J., … Scrivner, A. E. (2017). Radiocarbon constraints on the glacial ocean circulation and its impact on atmospheric $CO_2$. *Nature Communications*, *8*, 16010. https://doi.org/10.1038/ncomms16010

Sortor, R. N., & Lund, D. C. (2011). No evidence for a deglacial intermediate water $\Delta^{14}C$ anomaly in the SW Atlantic. *Earth and Planetary Science Letters*, *310*, 65–72. https://doi.org/10.1016/j.epsl.2011.07.017

St Laurent, L. C., Simmons, H. L., & Jayne, S. R. (2002). Estimating tidally driven mixing in the deep ocean. *Geophysical Research Letters*, *29*(23), 2106. https://doi.org/10.1029/2002GL015633

Stephens, B. B., & Keeling, R. F. (2000). The influence of Antarctic sea ice on glacial–interglacial $CO_2$ variations. *Nature*, *404*(6774), 171–174. https://doi.org/10.1038/35004556

Stott, L., & Timmermann, A. (2011). Hypothesized link between glacial/interglacial atmospheric $CO_2$ cycles and storage/release of $CO_2$-rich fluids from deep-sea sediments. In H. Rashid, L. Polyak, & E. Mosley-Thompson (Eds.), *Abrupt climate change: Mechanisms, patterns, and impacts*, *Geophysical Monograph Series* (Vol. 193, pp. 123–138). Washington, DC: American Geophysical Union. https://doi.org/10.1029/2010GM001052

Stott, L., Southon, J., Timmermann, A., & Koutavas, A. (2009). Radiocarbon age anomaly at intermediate water depth in the Pacific Ocean during the last deglaciation. *Paleoceanography*, *24*, PA2223. https://doi.org/10.1029/2008PA001690

Thiagarajan, N., Subhas, A. V., Southon, J. R., Eiler, J. M., & Adkins, J. F. (2014). Abrupt pre-Bølling-Allerød warming and circulation changes in the deep ocean. *Nature*, *511*(7507), 75–78. https://doi.org/10.1038/nature13472

Thornalley, D. J. R., Barker, S., Broecker, W. S., Elderfield, H., & McCave, I. N. (2011). The deglacial evolution of North Atlantic deep convection. *Science*, *331*, 202–205. https://doi.org/10.1126/science.1196812

van Geen, A., Fairbanks, R. G., Dartnell, P., McGann, M., Gardner, J. V., & Kashgarian, M. (1996). Ventilation changes in the northeast Pacific during the last deglaciation. *Paleoceanography*, *11*(5), 519–528. https://doi.org/10.1029/96PA01860

Wan, S., & Jian, Z. (2014). Deep water exchanges between the South China Sea and the Pacific since the last glacial period. *Paleoceanography*, *29*, 1162–1178. https://doi.org/10.1002/2013PA002578

Waterhouse, A. F., MacKinnon, J. A., Nash, J. D., Alford, M. H., Kunze, E., Simmons, H. L., … Lee, C. M. (2014). Global patterns of diapycnal mixing from measurements of the turbulent dissipation rate. *Journal of Physical Oceanography*, *44*(7), 1854–1872. https://doi.org/10.1175/JPO-D-13-0104.1

Wunsch, C. (2003). Determining paleoceanographic circulations, with emphasis on the Last Glacial Maximum. *Quaternary Science Reviews*, *22*(2-4), 371–385. https://doi.org/10.1016/S0277-3791(02)00177-4

Wunsch, C. (2006). *Discrete inverse and state estimation problems: With geophysical fluid applications*. Cambridge, UK: Cambridge University Press. https://doi.org/10.1017/CBO9780511535949